

RL-TR-95-267  
Final Technical Report  
December 1995



# OPTICALLY CONTROLLED SHF SATCOM ARRAY

Boeing Defense and Space Group

Greg L. Abbas

DTIC QUALITY INSPECTED 4

19960212 029

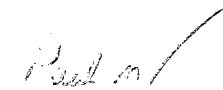
*APPROVED FOR PUBLIC RELEASE; DISTRIBUTION UNLIMITED.*

Rome Laboratory  
Air Force Materiel Command  
Rome, New York

This report has been reviewed by the Rome Laboratory Public Affairs Office (PA) and is releasable to the National Technical Information Service (NTIS). At NTIS, it will be releasable to the general public, including foreign nations.

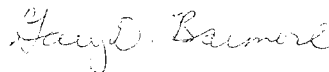
RL-TR-95-267 has been reviewed and is approved for publication.

APPROVED:



PAUL M. PAYSON  
Project Engineer

FOR THE COMMANDER:



GARY D. BARMORE, Major, USAF  
Deputy Director of Surveillance & Photonics

If your address has changed or if you wish to be removed from the Rome Laboratory mailing list, or if the addressee is no longer employed by your organization, please notify Rome Laboratory/ ( OCPC ), Rome NY 13441. This will assist us in maintaining a current mailing list.

Do not return copies of this report unless contractual obligations or notices on a specific document require that it be returned.

# REPORT DOCUMENTATION PAGE

Form Approved  
OMB No. 0704-0188

Public reporting burden for this collection of information is estimated to average 1 hour per response, including the time for reviewing instructions, searching existing data sources, gathering and maintaining the data needed, and completing and reviewing the collection of information. Send comments regarding this burden estimate or any other aspect of this collection of information, including suggestions for reducing this burden, to Washington Headquarters Services, Directorate for Information Operations and Reports, 1215 Jefferson Davis Highway, Suite 1204, Arlington, VA 22202-4302, and to the Office of Management and Budget, Paperwork Reduction Project (0704-0188), Washington, DC 20503.

1. AGENCY USE ONLY (Leave Blank)		2. REPORT DATE December 1995		3. REPORT TYPE AND DATES COVERED Final Sep 94 - Sep 95	
4. TITLE AND SUBTITLE  OPTICALLY CONTROLLED SHF SATCOM ARRAY				5. FUNDING NUMBERS C - F30602-94-C-0295 PE - 63726F PR - 2863 TA - 92 WU - 64	
6. AUTHOR(S)  Greg L. Abbas					
7. PERFORMING ORGANIZATION NAME(S) AND ADDRESS(ES) Boeing Defense and Space Group P.O. Box 3999, M/S 87-49 Seattle WA 98124-2499				8. PERFORMING ORGANIZATION REPORT NUMBER  N/A	
9. SPONSORING/MONITORING AGENCY NAME(S) AND ADDRESS(ES)  Rome Laboratory/OCPC 25 Electronic Pky Rome NY 13441-4515				10. SPONSORING/MONITORING AGENCY REPORT NUMBER  RL-TR-95-267	
11. SUPPLEMENTARY NOTES  Rome Laboratory Project Engineer: Paul M. Payson/OCPC/(315) 330-3144					
12a. DISTRIBUTION/AVAILABILITY STATEMENT  Approved for public release; distribution unlimited.				12b. DISTRIBUTION CODE	
13. ABSTRACT (Maximum 200 words)  Photonics technology offers many advantages when applied to phased array antenna problems. These advantages include small size, low weight, low loss, wide bandwidth, and advanced signal processing functions such as high-resolution, broadband, amplitude and phase control, variable true time delay, and broadband correlation for jammer nulling. This one-year study contract investigated the use of integrated optical circuits for high-resolution amplitude and phase control of super high frequency (SHF) signals. Airborne and space-based, transmit and receive phased array antennas were designed. The antenna designs are compatible with the Defense Satellite Communications System (DSCS) bands--7.25 to 7.75 GHz downlink and 7.9 to 8.4 GHz uplink.					
14. SUBJECT TERMS  Photonics, Phased array, Optically controlled satellite communications				15. NUMBER OF PAGES 68	
				16. PRICE CODE	
17. SECURITY CLASSIFICATION OF REPORT UNCLASSIFIED	18. SECURITY CLASSIFICATION OF THIS PAGE UNCLASSIFIED	19. SECURITY CLASSIFICATION OF ABSTRACT UNCLASSIFIED	20. LIMITATION OF ABSTRACT  UL		

# TABLE OF CONTENTS

1.0	SUMMARY .....	1
2.0	INTRODUCTION .....	3
2.1	Background .....	3
2.2	Objectives and Deliverables.....	6
2.3	Document Outline .....	6
3.0	STUDY RESULTS.....	7
3.1	True Time Delay Beam Steering.....	7
3.2	Conformal Airborne Aperture.....	8
3.3	Shared T/R Aperture.....	8
3.4	Optical Upconversion.....	8
3.5	Complex Weighted Optical Carrier Generation .....	10
3.6	Optical Downconversion .....	15
3.7	Phase and Amplitude Control With Integrated Optics.....	16
3.8	Techniques for Forming Single Beams.....	18
3.8.1	Transmit Antenna .....	18
3.8.2	Receive Antenna .....	19
3.9	Techniques for Forming Multiple Beams .....	20
3.9.1	Transmit Antenna .....	20
3.9.2	Receive Antenna .....	23
3.10	Jammer Nulling.....	25
3.11	Impact of Phase and Amplitude Errors .....	33
3.12	Choice of Optical Wavelength .....	37
3.13	Proof of Concept Demonstration.....	38
4.0	ANTENNA DESIGN OVERVIEW.....	44
4.1	Airborne Transmit.....	44
4.2	Airborne Receive .....	48
4.3	Space-Based Transmit.....	51
4.4	Space-Based Receive .....	54
5.0	CONCLUSIONS .....	57
6.0	REFERENCES .....	58

## LIST OF FIGURES

2.1-1	Airborne Transmit and Receive Antenna Application .....	5
2.1-2	Space-Based Transmit and Receive Antenna Application .....	5
3.1-1	Beam Squint Loss .....	7
3.4-1	An Optical Upconverter.....	8
3.4-2	Efficiency Comparison of Phase and Null-Biased MZ Modulators .....	9
3.4-3	Modulation Spectra of MZ Modulators at Quadrature and Peak Bias .....	10
3.5-1	Techniques for Generating RF Signals on Optical Carriers.....	11
3.5-2	More Techniques for Generating RF Signals on Optical Carriers .....	12
3.5-3	Modulation Efficiency Comparison.....	13
3.5-4	Modulation Spectrum and Waveform With Square Wave Distortion .....	14
3.5-5	Comparison of Modulation Techniques.....	14
3.6-1	Comparison of Optical Downconverter Techniques.....	15
3.7-1	Phase Control With Orthogonal Polarizations .....	16
3.7-2	Phase Control With a Single Polarization.....	17
3.8.1-1	Transmit Antenna Using IOC With Crossed Polarizations.....	18
3.8.1-2	Transmit Antenna Using IOC With Single Polarization.....	19
3.8.2-1	Receive Antenna Using Electronic Downconversion.....	19
3.8.2-2	Receive Antenna Using Optical Downconversion .....	20
3.9.1-1	Transmit Controller for Four Beams.....	21
3.9.1-2	Optical and Photocurrent Spectra Using a Null-Biased Mach-Zehnder .....	22
3.9.1-3	Optical and Photocurrent Spectra Using a Phase Modulator.....	22
3.9.2-1	Multiple Beam Receive Antenna With Electronic Downconversion.....	23
3.9.2-2	Multiple Beam Receive Antenna With Optical Downconversion.....	24
3.10-1	Null Depth Versus Fractional Bandwidth and Degrees of Freedom.....	26
3.10-2	Null Depth Versus Number of Nulls (Degrees of Freedom) .....	27
3.10-3	Array Configuration Used For Jammer Nulling Examples .....	28
3.10-4	Array Factor With Uniform Weighting .....	29
3.10-5	Jammer Nulling Example (3 Jammers and 6 Degrees of Freedom).....	29
3.10-6	Array Pattern Along the $V=0$ Axis Before (solid) and After (dashed) Adaptation.....	30
3.10-7	Null Bandwidths .....	30
3.10-8	Antenna Pattern With 40 dB Taylor Weighting and No Jammers.....	31
3.10-9	Adapted Pattern With 40 dB Taylor Weighting and Three Jammers .....	32

## LIST OF FIGURES

3.10-10	Array Pattern Along the $V=0$ Axis Before (solid) and After (dashed) Adaptation .....	32
3.11-1	Array Factor With Uniform Weighting .....	33
3.11-2	Array Factor With Taylor Weighting (40 dB, $\bar{n}=5$ ) .....	34
3.11-3	Effect of Amplitude and Phase Errors on Sidelobes .....	34
3.11-4	Array Pattern With a Single Adapted Null .....	35
3.11-5	Null Depth Limit With Phase and Amplitude Errors .....	36
3.12-1	Cost Comparison of Various Laser Sources .....	37
3.13-1	Four-Channel Phase Controller Integrated Optical Circuit .....	38
3.13-2	Optically Controlled Phased Array Test Apparatus .....	39
3.13-3	Miniature Anechoic Chamber (With Top Removed) .....	40
3.13-4	Antenna Patterns at -30 V, -20 V, and -10 V Steering Voltages .....	41
3.13-5	Antenna Patterns at 0 V, +10 V, and +20 V Steering Voltages .....	42
3.13-6	Antenna Pattern at +30 V Steering Voltage .....	43
3.13-7	Linear Tuning of Main Beam Angle With Steering Voltage .....	43
4.1-1	Performance Parameters for the Airborne Transmit Antenna .....	44
4.1-2	Airborne Transmit Antenna Block Diagram .....	45
4.1-3	Airborne Transmit Antenna EIRP Calculation .....	47
4.2-1	Performance Parameters for the Airborne Receive Antenna .....	48
4.2-2	Airborne Receive Antenna Block Diagram .....	49
4.2-3	Airborne Receive Antenna G/T Calculation .....	50
4.3-1	Performance Parameters for the Space-Based Transmit Antenna .....	51
4.3-2	Space-Based Transmit Antenna Block Diagram .....	52
4.3-3	Space-Based Transmit Antenna EIRP Calculation .....	53
4.4-1	Performance Parameters for the Space-Based Receive Antenna .....	54
4.4-2	Space-Based Receive Antenna Block Diagram .....	55
4.4-3	Space-Based Receive Antenna G/T Calculation .....	56

## TABLE OF ACRONYMS

DBS	direct broadcast satellite
DC	direct current
DSCS	Defense Satellite Communications System
EDM	exploratory development model
EHF	extremely high frequency
EIRP	effective isotropic radiated power
EME	electromagnetic effects
FDM	frequency division multiplexer
G/T	gain to temperature ratio
ICAPA	integrated circuit active phased array
IF	intermediate frequency
IOC	integrated optical circuit
LiNbO <sub>3</sub>	lithium niobate
LNA	low noise amplifier
LO	local oscillator
MMIC	microwave monolithic integrated circuit
MSSL	mean square sidelobe level
MZ	Mach-Zehnder
Nd:YAG	neodymium-doped yttrium aluminum garnet
PM	polarization maintaining
R&D	research and development
RF	radio frequency
RMS	root mean square
SATCOM	satellite communication
SHF	super high frequency
SM	single mode
SOW	statement of work
TBD	to be determined
T/R	transmit/receive
VTD	variable time delay

## 1.0 SUMMARY

This document is a final report describing work completed under a one-year contract (F30602-94-C-0295) awarded to Boeing by Rome Laboratory on 27 September 1994. The work accomplished was in accordance with the statement of work entitled "Optically Controlled SHF SATCOM Array" dated 31 August 1993, and is believed to completely satisfy the stated objectives of that statement of work. The objective of the contract was to develop designs for SHF (super high frequency) satellite communications antennas for airborne and space-based platforms utilizing photonics technology for beam formation (including multiple beams), true time delay beam steering, and beam control. The uplink and downlink frequency bands were 7.9 to 8.4 GHz and 7.25 to 7.75 GHz, respectively, for compatibility with the Defense Satellite Communications System (DSCS).

Photonics technology offers multiple advantages when applied to phased array antenna problems. When compared to radio frequency (RF) coaxial cables or waveguide, there are the advantages of:

- light weight,
- small size,
- low transmission loss,
- optical multiplexing,
- broad bandwidth,
- common component designs for multiple RF bands, and
- resistance to electromagnetic effects (EME).

These advantages come into play when signals must be transferred back and forth between the phased array controller and the phased array aperture. Future systems with higher transmission frequencies, broader bandwidths, and longer transmission distances further compound the photonic advantage.

The main focus of this contract is a less well known advantage of photonics technology, which is that photonics offers phased array antenna signal processing capabilities. These capabilities either are not available or are prohibitively expensive when implemented by purely electronic means. These signal processing functions include:

- high-resolution, broadband amplitude and phase control of RF signals,
- variable true-time delay, and
- broadband correlation for jammer nulling.

As an additional feature, many of these signal processing functions can be implemented so that the hardware design is independent of the actual RF antenna band. Thus, photonic signal processing module designs can be common to multiple applications, reducing future system cost and increasing functionality.



This contract investigated the application of photonic technology to airborne and space-based phased array antennas compatible with DSCS. The goal was to identify areas in the phased array design where it is advantageous and practical to apply photonic technology. Areas of particular interest for the application of photonics include:

- beam forming,
- beam steering,
- beam nulling,
- data control, and
- RF signal distribution.

Experimental demonstrations were performed and measured results are presented here that verify the feasibility of controlling phased array antennas using integrated optical techniques.

A system design plan was developed for both the airborne and space-based antennas. The design plan included system and module block diagrams, power budgets, and performance estimates. An overview of the design plan is included in this report.

For the DSCS application, the area where photonics technology can make the most significant contribution is with the space-based receive antenna. This antenna requires relatively tight tolerances on element phases and amplitudes in order to adapt and form deep nulls to reject unwanted jammers. Depending on the desired null depth, the required accuracies could be a few degrees of phase and a small fraction of a dB in amplitude across a channel bandwidth. Photonics technology offers a possibility of such accuracies over even broader bandwidths.

Phased array antennas with the following characteristics would increase the practicality and highlight the advantages of using photonics technology:

- large fractional bandwidths or multiband applications,
- multiple beam applications,
- large apertures,
- low sidelobe constraints,
- jammer nulling requirements, or
- extremely high RF center frequency with close element spacing.

The DSCS application offers the advantage of relatively low cost hardware so that large-scale photonically-controlled phased array antenna prototypes can be built to demonstrate the capabilities of the emerging technology. The frequency-independent nature of the integrated optical phase, amplitude, and true time delay control technology ensures that the results will extend to any RF band.

## 2.0 INTRODUCTION

### 2.1 BACKGROUND

All-electronic phased array designs have been developed for many systems. However, most of these systems are restricted to narrow bandwidth because of limitations on the microwave distribution network and electronic phase shifters. For wide-angle scanning, half-wavelength module spacing is necessary which severely restricts the cross-sectional area of the modules, particularly for the EHF band. The desire for thin antennas for either conformal or non-protrusive mounting limits the depth dimension of modules. The lack of available space constrains component sizes. Incorporating multiple signal channels for either multiband and/or multibeam operation, or for RF polarization control, becomes unrealistic. The problem is compounded if sidelobe suppression or beam nulling is required, because precise amplitude control must be included along with increased phase shifting precision.

The photonic beam control concepts described later offer an effective way to neutralize the limitations discussed above. Using a Boeing-pioneered photonic phase shifting technique, we are able to remove all control functions — phase shifting and amplitude weighting — from the antenna modules, as well as their companion logic circuits. This relaxes the size problem, simplifies the module design, and decreases power dissipation. Multiple beam control channels can be included in high-density, compact integrated optical circuit (IOC) modules. The implementation of parallel beam-forming networks for multibeam and multi-frequency operation becomes practical. Optionally, this technology also allows dual channels per module for microwave polarization control.

Equally important for some applications, our microwave-frequency-independent photonic control devices are capable of very high precision. Using the linear electrooptic effect of  $\text{LiNbO}_3$ , extremely linear phase shifts can be achieved over a broad RF bandwidth. Furthermore, phase shifts and amplitude controls are uncoupled, unlike conventional MMIC phase shifter designs with limited bit resolution and non-uniform loss for each phase setting. This operation is essential for high-performance beam forming applications such as low sidelobe control.

Boeing has been aggressively developing photonic components and techniques for wideband analog applications, especially phased arrays. Our approach centers on low-loss, compact IOCs that incorporate many phased array control functions on a common substrate using a mature  $\text{LiNbO}_3$  fabrication process. Using this approach, we have demonstrated phased array beamsteering in both transmit and receive modes from 20 to 40 GHz, and automatic target tracking with a single, frequency-independent, optical phase shifter IOC. We have also demonstrated a compact 3-bit optical variable-time delay (VTD) module. This photonic approach provides important new tools to improve phased array antenna performance.

Boeing is an established leader in active phased arrays for EHF communications. Under the Integrated Circuit Active Phased Array (ICAPA) contract (F19628-90-C-0168) with Rome Laboratory, we delivered 91-element subarrays at 20 GHz (receive) and 44 GHz (transmit). We are now expanding our phased array technology to commercial applications. A major internal initiative program toward advanced, yet practical, next-generation phased arrays was recently launched to fabricate a thin, superficially mountable phased array antenna of several thousand elements to provide in-flight reception of digital DBS (12.2 to

12.7 GHz) television signals on commercial airplanes. Low cost — in acquisition, installation, aerodynamic drag, and maintenance — is of paramount importance.

Photonics technology offers multiple advantages when applied to phased array antenna problems. When compared to coaxial cables or RF waveguide, there are advantages of:

- light weight,
- small size,
- low transmission loss,
- optical multiplexing,
- broad bandwidth,
- common link designs for multiple RF bands, and
- resistance to electromagnetic effects (EME).

These advantages come into play when signals must be transferred back and forth between the phased array controller and a possibly remote phased array aperture. Future systems with higher transmission frequencies, broader bandwidths, and longer transmission distances further compound the photonic advantage.

This contract investigated the application of photonic technology to airborne and space-based phased array antennas compatible with the Defense Satellite Communication System (DSCS). The goal of the design was to identify areas in the phased array design where it is advantageous and practical to apply photonic technology. Areas of particular interest for the application of photonics include:

- beam forming,
- beam steering,
- beam nulling,
- data control, and
- RF signal distribution.

Illustrations of the DSCS application addressed in this design plan are shown in Figures 2.1-1 and 2.1-2. The DSCS system uses the bands 7.25 to 7.75 GHz for downlink and 7.90 to 8.40 GHz for uplink. The bands are divided into six channels separated by guard bands. The maximum instantaneous bandwidth for a single channel is 85 MHz.

The airborne transmit and receive antennas consist of 256 elements each. The radiators are circularly polarized. The conical scan range of the array is 75°. The arrays can scan and reconfigure to maintain the communication link during maneuvers. The transmit array has an effective isotropic radiated power of +47 dBW. The receive array has an element noise figure of 6 dB. The airborne transmit and receive arrays provide for a single antenna beam carrying a single information channel at any one time.

The space-based transmit and receive antennas also consist of 256 elements each. The radiators are circularly polarized. Either antenna can produce up to four simultaneous independent beams. Each of the four beams is adjustable for either spot coverage or full-earth coverage. The spot beams can be independently pointed anywhere on the visible earth's surface. Any of the four beams can transmit or receive on any of the six DSCS channels. The space-based antenna elements can have  $2\lambda$ -spacing because of the limited scan range requirement. The space-based transmit antenna has a required EIRP of +50 dBW for each spot beam. The space-based receive antenna has an element noise figure of less than 6 dB. The

receive antenna has the additional requirement that it be able to adapt and suppress up to three simultaneous jammers.

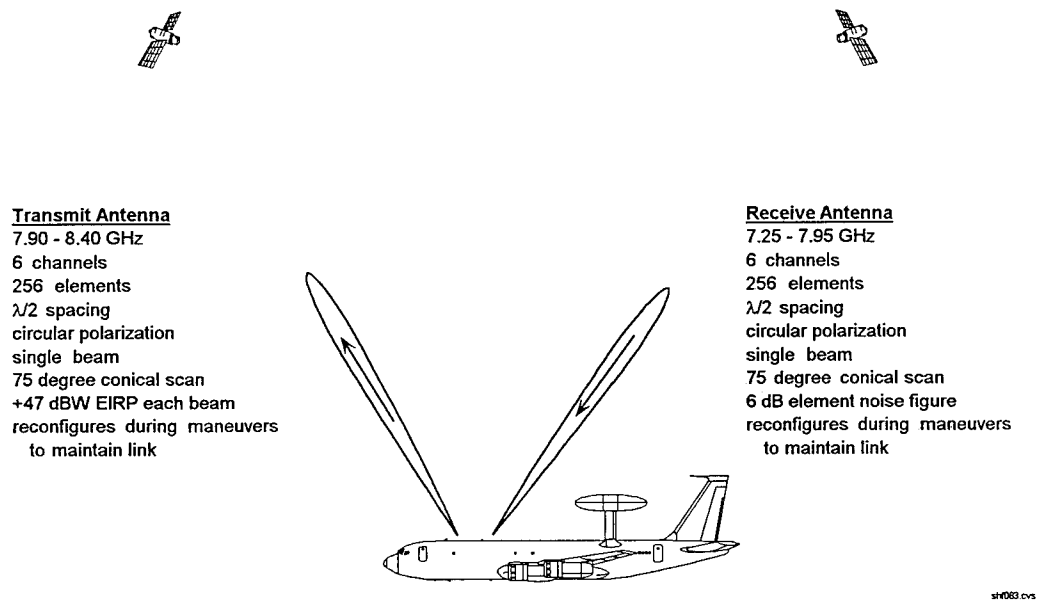


Figure 2.1-1. Airborne Transmit and Receive Antenna Application

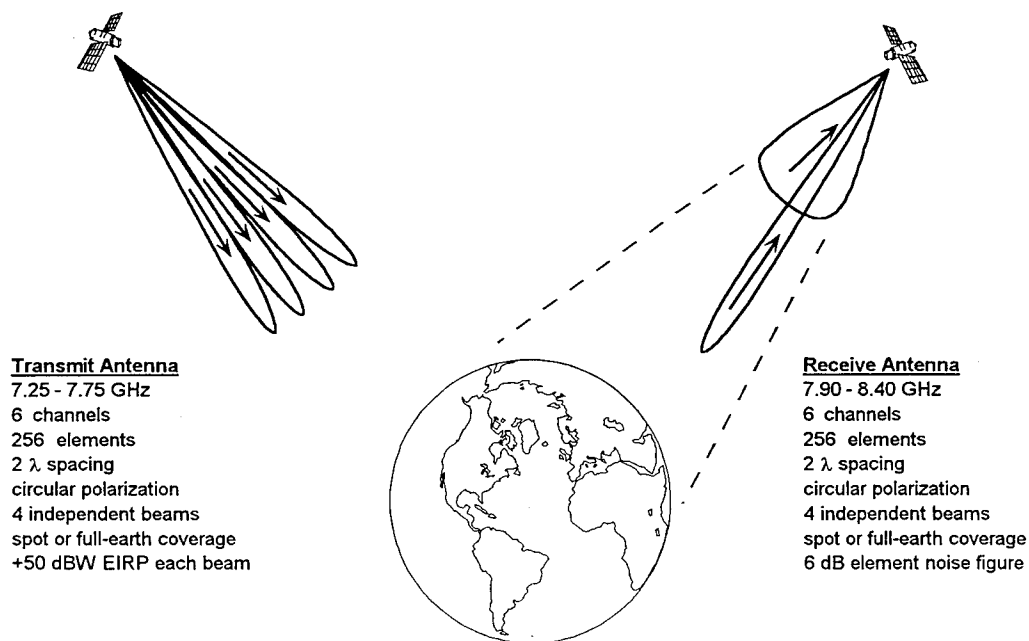


Figure 2.1-2. Space-Based Transmit and Receive Antenna Application

## **2.2 OBJECTIVES AND DELIVERABLES**

The objective of the contract was to develop designs for a super high frequency (SHF) satellite communications (SATCOM) antenna for airborne and space-based applications (7.25 to 7.75 GHz downlink and 7.9 to 8.4 GHz uplink) which utilize novel photonics technology for beam formation (including multiple beams), true time delay beam steering, and beam control. Laboratory experiments were to be conducted to verify concepts.

The Government's intent was to utilize the completed design information to prepare a statement of work (SOW) for a future effort involving fabrication of a proof of concept exploratory development model (EDM).

Documents delivered under the contract included:

1. Monthly research and development (R&D) status reports
2. Oral presentation materials
3. System design plan
4. Final scientific and technical report

No hardware was delivered under this contract.

## **2.3 DOCUMENT OUTLINE**

Section 3 presents the analysis and results obtained under this contract. Areas of study included true time delay beamsteering, conformal apertures, shared transmit/receive (T/R) apertures, optical upconversion, complex-weighted optical carrier generation, optical downconversion, phase and amplitude control of microwave signals using integrated optics, techniques for forming single and multiple beams, jammer nulling, phase and amplitude error effects, and the choice of optical wavelength. Experimental results demonstrating proof of the concept are presented. Section 4 gives a brief overview of the antenna system design plan. For a full discussion, refer to the system design plan document submitted under this contract and dated 25 September 1995. Finally, Section 5 gives overall conclusions drawn from the study.

### 3.0 STUDY RESULTS

#### 3.1 TRUE TIME DELAY BEAM STEERING

True time delay beam steering was considered for use in the airborne arrays because of the large scan angle requirement (75°). Boeing believes that true time delay processing is not required for this application with the standard DSCS III frequency plan. The 3 dB fractional bandwidth limited by beam squint is

$$\frac{\Delta f}{f} = 0.886 \cdot B_b \cdot \left[ \frac{\lambda}{L \cdot \sin(\theta_o)} \right],$$

where  $B_b$  is the beam broadening factor due to aperture weighting,  $\lambda$  is the RF wavelength,  $L$  is the array width, and  $\theta_o$  is the maximum steering angle. Using parameters for the airborne array with uniform weighting ( $B_b = 1$ ,  $L/\lambda = 8$ , and  $\theta_o = 75^\circ$ ) yields  $\Delta f/f = 11\%$  before squint becomes a (3 dB) problem. The worst case DSCS III channel gives 85 MHz / 7500 MHz = 1.1%. If one assumes that future wideband DSCS uses a full 500 MHz instantaneously, 500 MHz / 7500 MHz = 6.7%. Even this case is only a slight (1 dB) problem. However, true time delay would be required in future systems if larger antennas (relative to a wavelength) or more instantaneous fractional bandwidth were used.

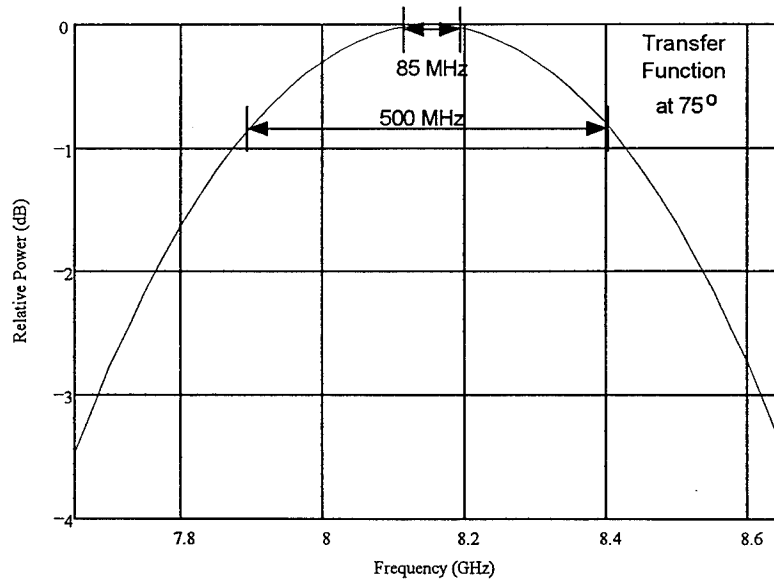


Figure 3.1-1. Beam Squint Loss

### 3.2 CONFORMAL AIRBORNE APERTURE

Boeing has investigated the issue of using conformal apertures as opposed to planar apertures. For this application, the transmit and receive apertures are about 14 inches in diameter. On a large airframe, such as the E3A, Boeing believes that the benefit in reduced drag obtained by using a conformal array is outweighed by the resulting increased cost and complexity. Boeing is presently designing a direct broadcast satellite (DBS) receive phased array antenna. The DBS antenna is larger in area than the airborne designs under consideration for this contract and is intended for use on large commercial aircraft. The DBS antenna has a planar design.

### 3.3 SHARED T/R APERTURE

The airborne antennas designed for this contract are relatively small — about 14 inches in diameter. The target airframe is a large aircraft such as the E3A. Boeing believes that the advantage of using a shared T/R aperture is outweighed by the additional complexity and performance penalties associated with T/R modules. We believe that sufficient room is available on the airframe to allow for physical separation of the transmit and receive apertures without excessive blockage by the radome or tail.

### 3.4 OPTICAL UPCONVERSION

Figure 3.4-1 shows a technique for using optics to translate an intermediate frequency (IF) input signal to an RF output. This technique can be used for transmit to map the IF information up to the transmission band. It can also be used for receive to generate an agile local oscillator signal such as might be required for spread spectrum signaling. Two single frequency lasers are stabilized at frequencies  $f_1$  and  $f_2$ . The output from laser #2 is phase or intensity modulated with an IF signal centered at  $f_{IF}$ . No bias control is required with phase modulation. An intensity modulator could be biased at quadrature, peak, null, or somewhere in between. The modulated signal is combined with the output from laser #1 and sent to a photodiode. The photodiode detects the optical signal and generates an RF photocurrent output.

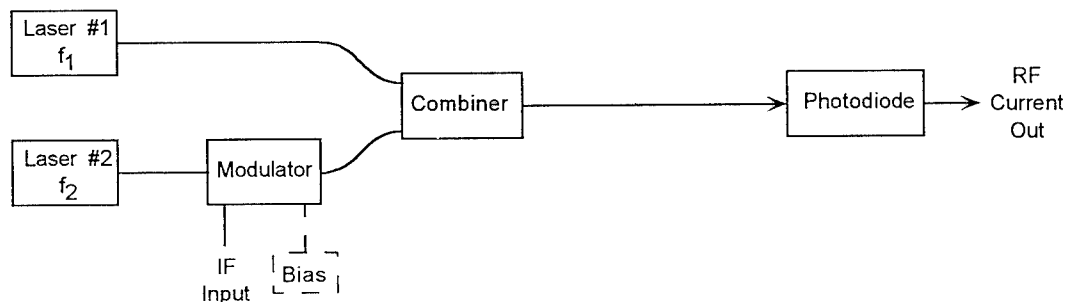


Figure 3.4-1. An Optical Upconverter

Figures 3.4-2 and 3.4-3 show power spectra of the optical fields and photodetector currents for an example with  $f_2 - f_1 = 7$  GHz and  $f_{IF} = 1$  GHz. The left side of Figure 3.4-2 shows the result of using a phase modulator. Phase modulation generates multiple harmonics in the optical field of laser #2 as shown centered about 7 GHz. The horizontal axis has been normalized to set  $f_1$  at 0 GHz. The photocurrent

spectrum is also shown. Many signals are generated in the photocurrent output. The only signal of interest is the +1 sideband at 8 GHz. All other signals must be filtered out.

The optical and photocurrent spectra generated by using a push-pull Mach-Zehnder modulator are shown in the right half of Figure 3.4-2. The optical spectrum has exactly the same level for the odd modulation harmonics of laser #2. The even harmonics are nulled. The photocurrent spectrum shows the same pattern. The advantages of using a null-biased push-pull Mach-Zehnder modulator are equal IF to RF modulation efficiency and an output with fewer spurious signals. One disadvantage is that a bias control circuit may be required to hold the modulator at the null with temperature changes. Second, the nulls in practice are not perfect, so the even harmonic spurs will still be present at some level..

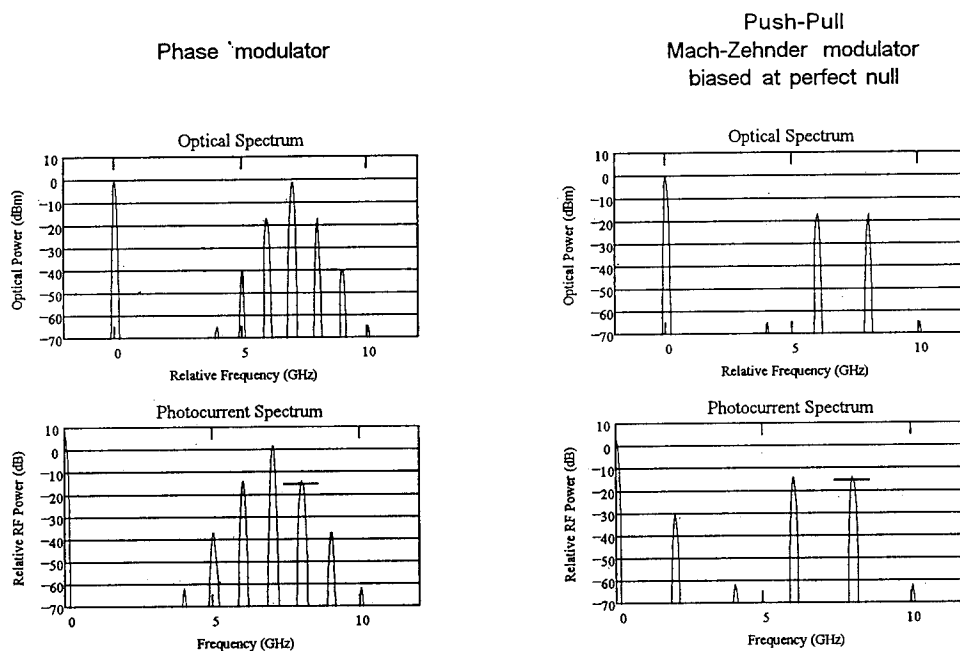


Figure 3.4-2. Efficiency Comparison of Phase and Null-Biased MZ Modulators

For completeness, the results for using a push-pull Mach-Zehnder modulator at quadrature and at peak bias are shown in Figure 3.4-3. The optical spectrum for the quadrature-biased case looks similar to the phase modulator result except that the +1 sideband is 3 dB lower. Biasing at the peak nulls the odd harmonics and leaves none of the desired +1 sideband.



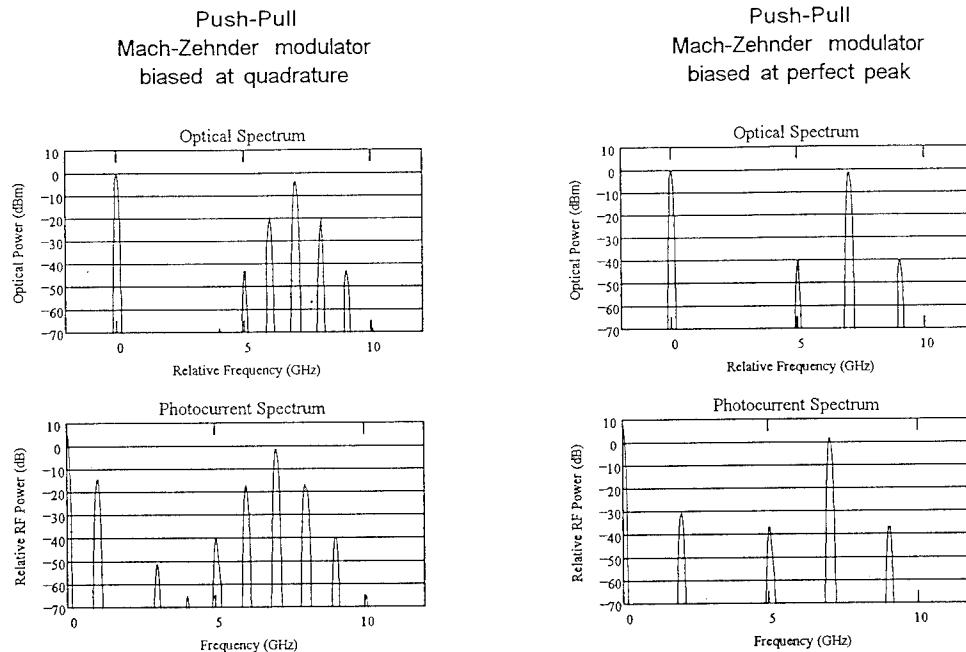


Figure 3.4-3. Modulation Spectra of MZ Modulators at Quadrature and Peak Bias

### 3.5 COMPLEX WEIGHTED OPTICAL CARRIER GENERATION

Figures 3.5-1 and 3.5-2 show four approaches for generating 256 complex-weighted optical carriers with independent control. A complex-weighted optical carrier is one whose phase and amplitude is controlled relative to a second optical carrier. For a receive array, the carriers are used to generate complex-weighted local oscillators for downconverting the received signals from each element. For transmit, these techniques can be used to adjust the phase and amplitude of the signals transmitted from individual elements.

The first technique (A) uses a Mach-Zehnder modulator to directly modulate the optical carrier with the desired local oscillator signal.<sup>1</sup> This technique has the advantage that only a single laser is required, and that the laser does not need to have particularly low phase noise. The disadvantage is that high speed modulators are required for each element. For the receive case and for some transmission formats where only discrete tones are required, the Mach-Zehnder modulator can be biased at the null and used to generate a frequency-doubled output.

A second issue is that the phase and amplitude weights are applied electronically to the modulator drive signal. This approach might make sense if RF amplitude and phase controllers are very inexpensive but too large to insert at the elements — possibly the case at EHF.

<sup>1</sup> Semiconductor modulators could also be used. They are smaller in size, but higher insertion loss at present.

The second approach (B) shown in Figure 3.5-1 uses two lasers that are phase locked with the desired frequency offset. The phase locking circuitry is fairly straight forward when using diode-pumped Nd:YAG's for the laser sources. Diode-pumped Nd:YAG's have extremely low phase noise compared to semiconductor lasers. Diode lasers have been phase locked, but the circuitry is considerably more complex. Unfortunately, diode-pumped Nd:YAG's are more expensive, larger, and have lower wall-plug efficiency than diode lasers.

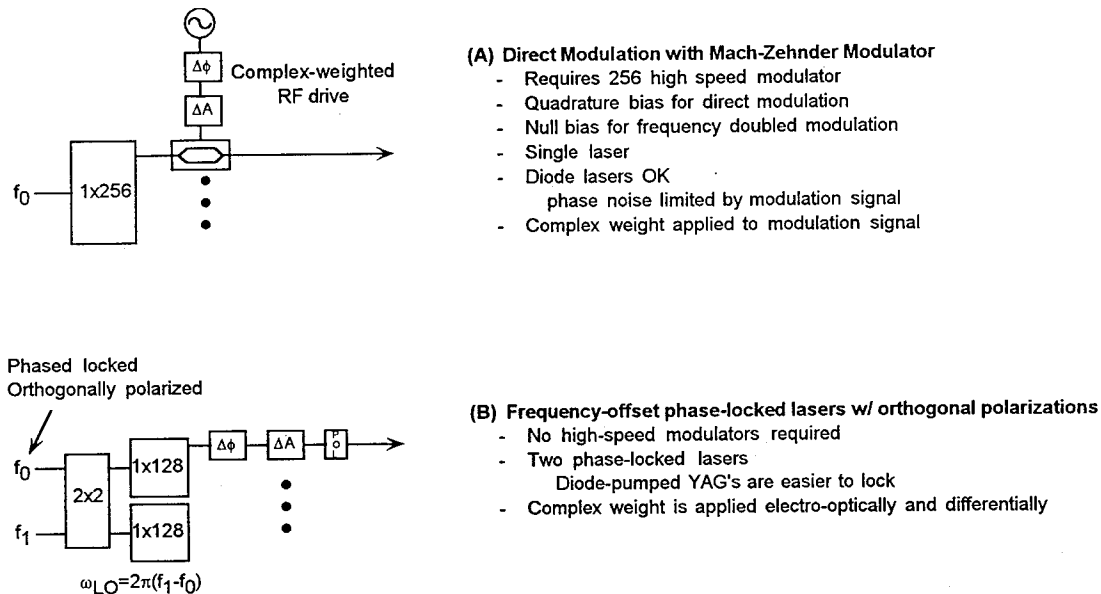


Figure 3.5-1. Techniques for Generating RF Signals on Optical Carriers

For approach (B), the complex weights are applied electro-optically as described in a later section. Phase is applied with a polarization sensitive phase modulator. Amplitude weighting is applied with a Mach-Zehnder modulator to one or both polarizations.

Figure 3.5-2 shows two more techniques for generating a complex-weighted optical carrier. These two approaches have advantages for systems where the LO frequency must be quickly retuned, such as with a frequency-hopped spread-spectrum receiver.

Approach (C) starts with two phase locked lasers. One of the lasers is modulated by an IF signal with a Mach-Zehnder modulator biased at the null. This technique was discussed in the previous section. The modulation creates primarily first-order sidebands offset from  $f_0$  by the modulation frequency. The two lasers signals are merged with orthogonal polarizations in a polarization combiner. After the combiner, the beam is split 256 ways and the individual complex amplitude and phase weights are applied.

Approach (C) has the advantage that only a single modulator is required. The modulator only needs to operate in the IF band — not the RF band. This is particularly an advantage at EHF.

Approach (D) in Figure 3.5-2 uses only a single laser. This time the optical carrier is modulated with an IF equal to half of the desired transmit frequency. This creates first-order sidebands separated by the transmit frequency. An optical frequency division multiplexer (FDM) is used to separate the two sidebands into

separate channels. One of the sidebands is rotated in polarization, and the two sidebands are recombined with a polarization combiner. The subsequent splitting and complex weighting is identical to the previous cases.

This approach requires locking the laser to the FDM so that the sidebands are properly separated. An advantage of this approach is that it may be possible to use diode lasers. A possible problem is that the FDM will put a bandwidth limit on the IF modulation. If the IF changes too much, the FDM splitting will not be clean.

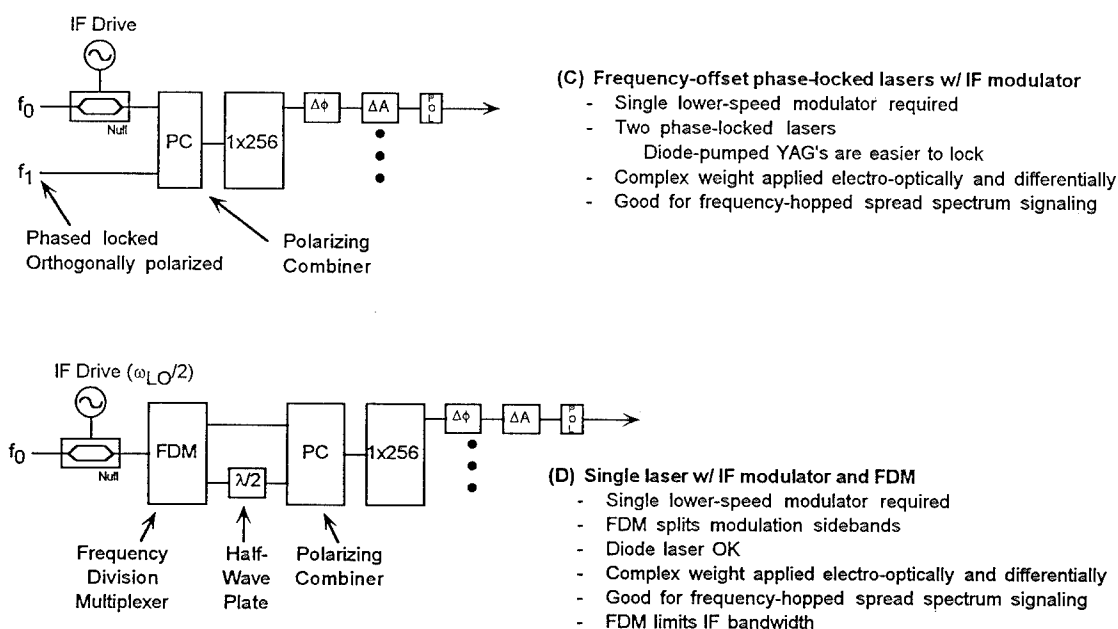


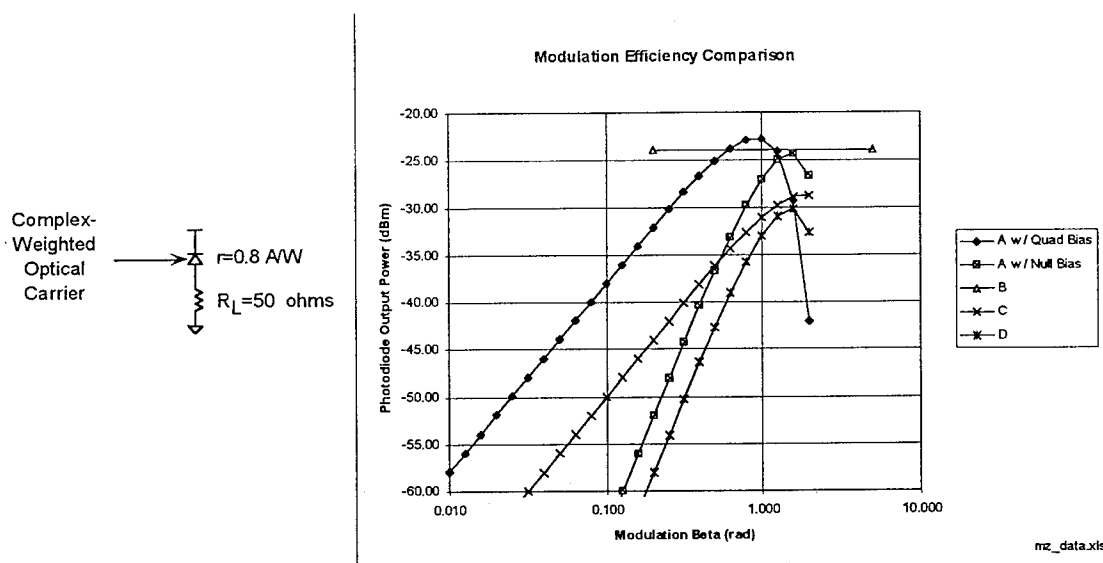
Figure 3.5-2. More Techniques for Generating RF Signals on Optical Carriers

A comparison of the modulation efficiencies of the two schemes is shown in Figure 3.5-3. For the direct Mach-Zehnder modulation approach (A), we start with 256 mW of optical power. This is immediately split 256 ways so that there is 1 mW of laser power per element. Assume that the modulator is biased at quadrature. Ignoring insertion losses, the average optical power out of the modulator is 0.5 mW. The photodiode has a responsivity of 0.8 A/W. The DC photocurrent is 0.4 mA. The load resistance is 50  $\Omega$ . Figure 3.5-3 shows the RF power delivered to the load resistor as a function of the modulator drive level,  $\beta$ , defined as:

$$\beta = \pi \cdot \frac{V_{IN}}{V_{\pi, PM}}$$

$V_{IN}$  is the input voltage to the modulator.  $V_{\pi, PM}$  is the voltage required to phase shift one arm of the modulator by 180°. Note that  $V_{\pi}$  for a push-pull Mach-Zehnder modulator is one-half of  $V_{\pi, PM}$ . For approach (A), the peak RF output power occurs when  $\beta$  is about 0.92. This is equivalent to driving the modulator slightly beyond peak to null. The modulated optical spectrum and photocurrent waveform are

shown in Figure 3.5-4. The small signal slope is 20 dB per decade. The maximum output power is about -22.7 dBm.



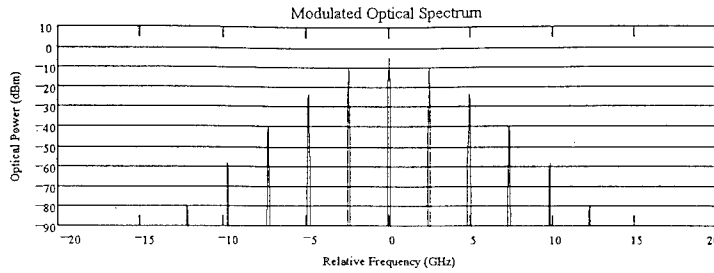
For all cases: Total laser power is 256 mW (1 mW per element), responsivity is 0.8 mA/mW, load resistance is 50 ohms  
 → Photodiode impedance matching may give several dB improvement

Figure 3.5-3. Modulation Efficiency Comparison

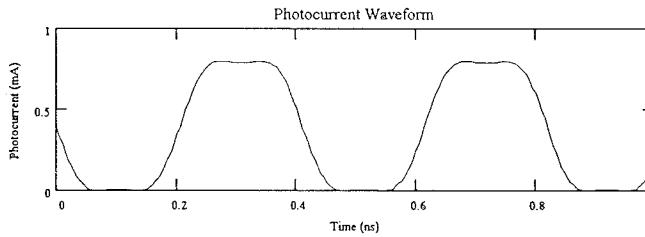
Now consider the case where the Mach-Zehnder modulator is biased at null (approach A w/ null bias). A frequency-doubled version of the drive signal is generated at the photodiode. The strength of the second harmonic power is shown in Figure 3.5-3. For small signals, the gain is 40 dB per decade. The signal output power saturates at a drive level of about  $\beta = 1.53$  and an output power of -24.2 dBm. Thus, to use the modulator as a frequency doubler by biasing at the null requires somewhat larger drive levels and is slightly less efficient.

Approach (B) for generating a complex weighted optical carrier is to use two frequency-offset phase locked lasers. To make the comparison fair, we start with 128 mW for each laser. With no insertion losses, the optical power after the polarizer is 0.5 mW per element. We again end up with 0.4 mA DC photocurrent. The balanced laser powers give a 100% modulation depth, so the photocurrent swings sinusoidally between 0.0 and 0.8 mA. This delivers -24.0 dBm to the load resistance, as shown by the flat line in Figure 3.5-3.

At first thought, one might assume that the approach (B) with the phase-locked lasers and 100% modulation depth would be maximally efficient. However, this is not the case. The near square-wave distortion produced by the overdriven Mach-Zehnder modulator produces a fundamental component in the photocurrent with a larger amplitude than the DC component of the photocurrent. The fundamental Fourier component of a square wave has a peak-to-peak amplitude larger than the peak-to-peak amplitude of the square wave itself.



Many harmonics generated  
in optical spectrum



RF drive is slightly beyond peak-to-null

Figure 3.5-4. Modulation Spectrum and Waveform With Square Wave Distortion

Similar results are shown for approaches (C) and (D). For (C), we start with 128 mW per laser. With (D), we start with 256 mW. The optimal modulation levels and peak output powers for each scheme are shown in Figure 3.5-5.

	peak $\beta$	peak $P_{out}$
A w/ quad bias	0.92	-22.7
A w/ null bias	1.53	-24.2
B		-24.0
C	1.84	-28.7
D	1.84	-30.2

Figure 3.5-5. Comparison of Modulation Techniques

In summary, approach (A) with a Mach-Zehnder modulator for each element has the best efficiency, but is probably too expensive. Approach (B) is the simplest and next most efficient. It is the probably the best approach for an SHF DSCS-band receiver. Approaches (C) and (D) are less efficient, but suitable for applications where fast tuning of the local oscillator is required (for example, frequency-hopped spread spectrum).

### 3.6 OPTICAL DOWNCONVERSION

Figure 3.6-1 indicates several levels of penetration of the optical signal into the receiver down-converter. The first example shows the complex-weighted optical local oscillator (LO) being converted to an electrical LO. The mixing and summing functions are done electrically. We expect that electrical mixing and summing is the lowest cost, size, and risk solution in the near term. This may be the best solution for the SHF airborne receive application. The difficulty arises with the space-based receive application, where broadband jammer nulling is a requirement. In order to form a deep, broadband null, all of the components in the received signal chain must be carefully matched. The matching requirement depends on the desired level of nulling. Amplitude and phase matching may need to be better than a fraction of a dB and a few degrees. This is difficult with a chain of several broadband RF and IF components.

The second example shows the mixing being done electro-optically with a Mach-Zehnder modulator, followed by electrical summing. The output of the photodiode contains a component that is the product of the received signal and the complex-weighted optical LO. High-speed MZ modulators and photodiodes are available that have bandwidths greater than 40 GHz. Thus, at SHF, it may be simpler to match the MZ and photodiode than it is to match the RF mixer, especially over the relatively small DSCS bandwidth of 500 MHz centered near 8 GHz. Electro-optic mixing has a second advantage in that it is suitable for applying multiple complex weights to form multiple beams in a single operation. As discussed in Section 3.9, this is accomplished by using separate complex-weighted LO's for each beam. These are all multiplied with the received signal at once to produce multiple complex-weighted IF signals. This type of operation could also be done electronically if the mixer was used as a linear multiplier as opposed to being operated in a saturated mode.

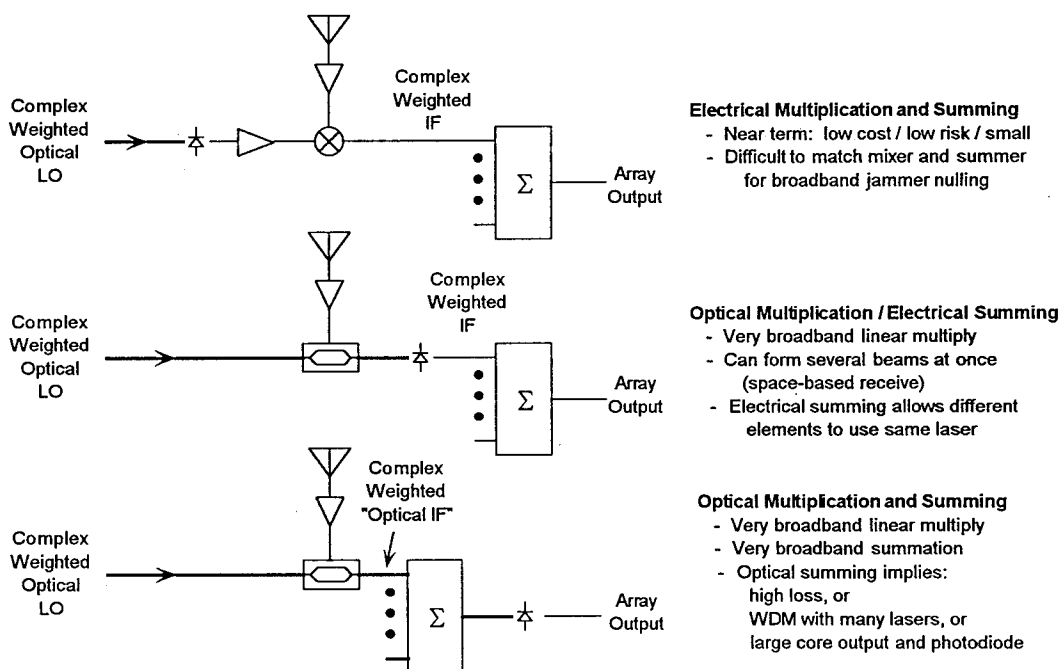


Figure 3.6-1. Comparison of Optical Downconverter Techniques

The final case shows the mixing and summing both being done optically. This is the technique used in recent work at Lincoln Lab (ref. 1). The outputs of the MZ modulators are combined onto a single photodiode. This approach gives an additional constraint that the lasers for each element must be widely separated in frequency. Otherwise, unwanted beat signals will be produced in the photodiode that might interfere with the desired signal. A second problem is that optical combining is usually not very efficient. The photodiode must be fairly small ( $\sim 100 \mu\text{m}$  diameter), or it will not be able to respond to the desired signal. The output of the MZ modulator can be in single-mode fiber ( $\sim 10 \mu\text{m}$  diameter core). A standard single-mode Nx1 combiner has a combining loss of  $1/N$ . This is very lossy when  $N$  is large. Apparently, Lincoln Lab used a single-mode to multi-mode combiner that is fairly efficient, but limited to a small number of inputs. We feel that this approach is not extendible to a large number of elements, particularly with wide bandwidth signals that will require small photodiodes. A two-stage design, with optical summing of elements within a subarray and electrical summing of subarrays, may be better.

### 3.7 PHASE AND AMPLITUDE CONTROL WITH INTEGRATED OPTICS

Integrated optical devices can be used to control the phase and amplitude of the microwave beat signals generated by the optical upconversion techniques discussed in the previous sections. Figure 3.7-1 shows one approach. Two lasers are locked at frequencies  $f_1$  and  $f_2$ . The two optical carriers are input to the integrated optical controller with orthogonal polarizations as shown in the figure. When a voltage is applied to the electrode on the device, an index change occurs in the crystal. The index change is different for the two polarizations. The index changes lead to a differential phase shift between the two optical carriers. In order to generate a heterodyne beat signal, a polarizer is placed between the integrated optical controller and the photodiode. The axis of polarizer must be rotated  $45^\circ$  relative to the integrated optical device axes for maximum efficiency.

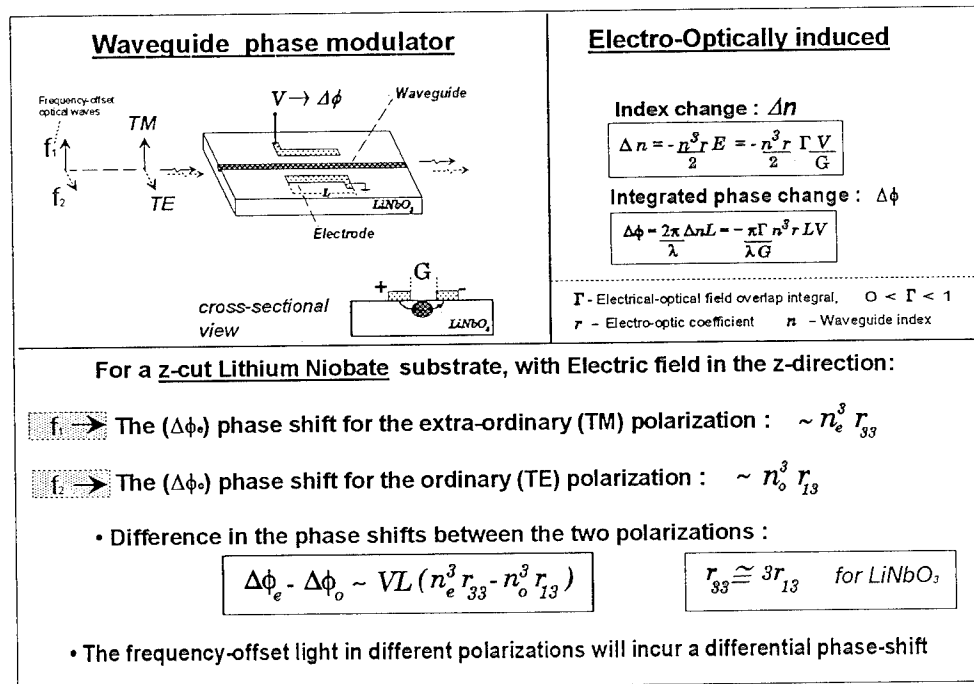


Figure 3.7-1. Phase Control With Orthogonal Polarizations

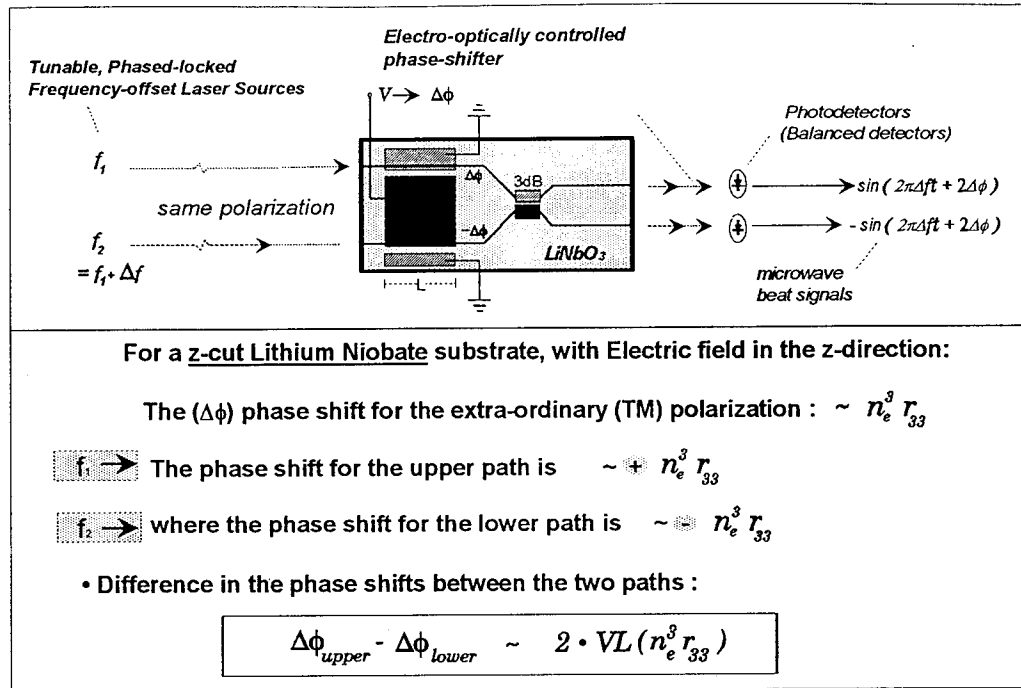


Figure 3.7-2. Phase Control With a Single Polarization

Figure 3.7-2 shows a second approach for controlling the microwave phase. Again, two lasers are locked with a fixed frequency separation. In this case, however, the optical carriers are input to the integrated optical controller with the same polarization but in different waveguides. The two carriers are differentially phase shifted and then combined in a 3 dB coupler. The phase shift is about three times as sensitive to the electrode voltage as for the orthogonal polarization approach. This can be seen from the equations in the figures since the extraordinary index  $n_e$  is approximately equal to ordinary index  $n_o$  and the  $r_{33}$  coefficient is three times as large as  $r_{13}$ . The output from the device has two ports that will produce beat signals on a photodiode. The beat signals are  $180^\circ$  out of phase.

The orthogonal polarization approach has the advantage that the two carriers travel along the same path through the device. This minimizes common mode effects such as temperature gradients across the device. Disadvantages are that the control voltages are three times as large and the controlled phase accuracy is sensitive to the polarization purity at the input of the device. The second approach can avoid the potential polarization problem by using proton exchange to form the waveguides. Waveguides formed with this process only guide one polarization, guaranteeing a clean polarization. Another advantage of the single polarization approach is that a polarizer is not required to form the microwave beat signal on the photodiode. Rather than throwing away half of the optical power, the single polarization approach can use both optical outputs with a balanced optical receiver to maximize the optical efficiency.

It is also possible to control the amplitude of the microwave beat signal by using another integrated optical device such as a Mach-Zehnder modulator. The Mach-Zehnder can be integrated into the same substrate as the phase controller and adjusts the amplitude of one or both of the optical carriers.



## 3.8 TECHNIQUES FOR FORMING SINGLE BEAMS

### 3.8.1 Transmit Antenna

The architecture shown in Figure 3.8.1-1 shows how the upconversion technique and the integrated optical phase and amplitude controls of the previous sections can be applied to a phased array antenna. Optical carriers are locked at frequencies  $f_0$  and  $f_1$ . The  $f_1$  carrier is modulated to produce multiple optical sidebands. The two carriers are combined in the integrated optical controller and adjusted in phase and amplitude to set the desired complex weight. In the antenna module, the optical carriers are photodetected. This produces several upconverted RF signals. The desired signal is selected by filtering, amplified, and radiated. Many phase and amplitude weights can be applied with a single small integrated optical controller.

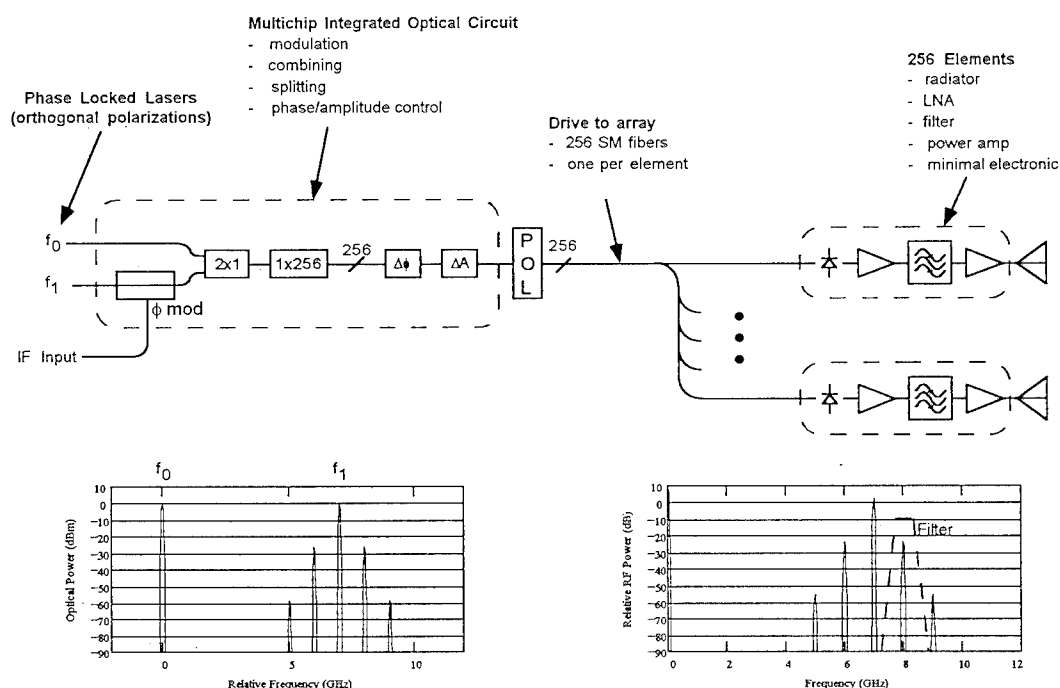


Figure 3.8.1-1. Transmit Antenna Using IOC With Crossed Polarizations

Figure 3.8.1-2 shows a slightly different approach for the integrated optical controller. For this case, the two optical carriers are kept separate while the phase and amplitude adjustments are applied. The two carriers are combined at the output of the integrated optical controller. As discussed in the previous section, this second approach has several advantages. The electrode voltage to phase sensitivity is improved by about a factor of three. Another advantage is that no polarizer is required at the output of the controller. Finally, single polarization optical waveguides can be used in the controller, minimizing effects due to polarization crosstalk. The disadvantage is that this approach may be more sensitive to temperature gradients across the device.

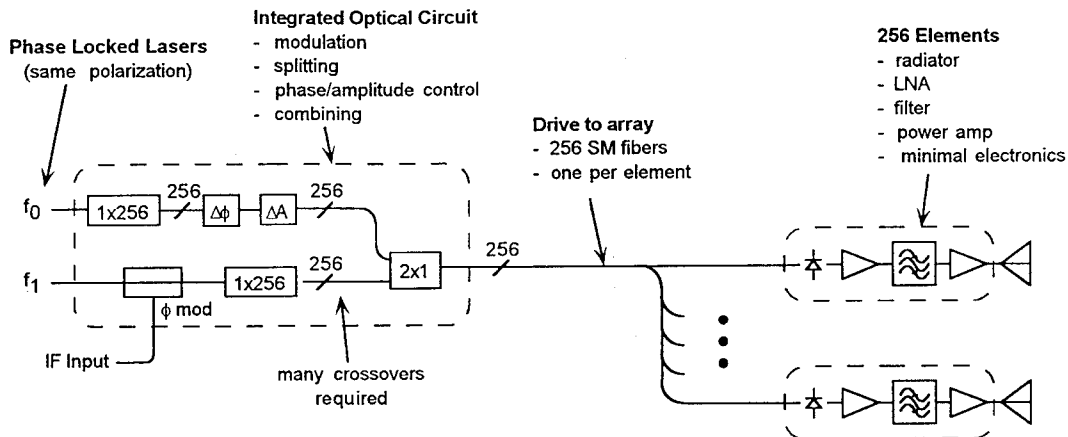


Figure 3.8.1-2. Transmit Antenna Using IOC With Single Polarization

### 3.8.2 Receive Antenna

Figure 3.8.2-1 shows an approach for forming a receive beam using an integrated optical controller and electronic downconversion. For this case, the integrated optical controller provides a phase-shifted local oscillator to each element. No amplitude weighting is provided. The controller is shown as using two orthogonally polarized optical carriers. It could also be implemented with a single polarization controller, if desired. In the antenna module, the received RF signal is mixed with the optically generated local oscillator to form a phase-shifted IF signal. The phase-shifted IF signals are summed. The figure shows the combined IF signal being returned to the array processor on another IF fiber optic link.

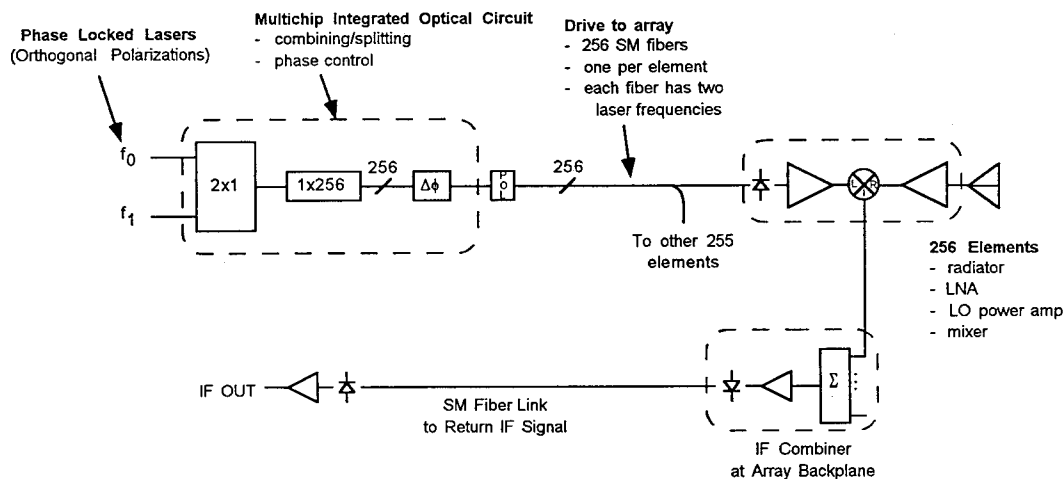


Figure 3.8.2-1. Receive Antenna Using Electronic Downconversion

Figure 3.8.2-2 shows an approach using optical downconversion. The two optical carriers are adjusted in amplitude and phase by the integrated optical controller. At the antenna element, the received RF signal is modulated onto the pair of carriers. A mixed down IF signal is produced at the photodetector. The complex-weighted IF signals are combined to form the receive beam. This approach has the advantage that

both phase and amplitude weighting can be applied during the downconversion. Optical weighting gives the possibility of better channel tracking for jammer nulling applications. The drawback is that an optical modulator operating at the RF frequency is required in each element.  $\text{LiNbO}_3$  modulators may be too large to include in the antenna modules, particularly for future EHF systems. At the present time, semiconductor modulators are sufficiently small, but have high insertion loss.

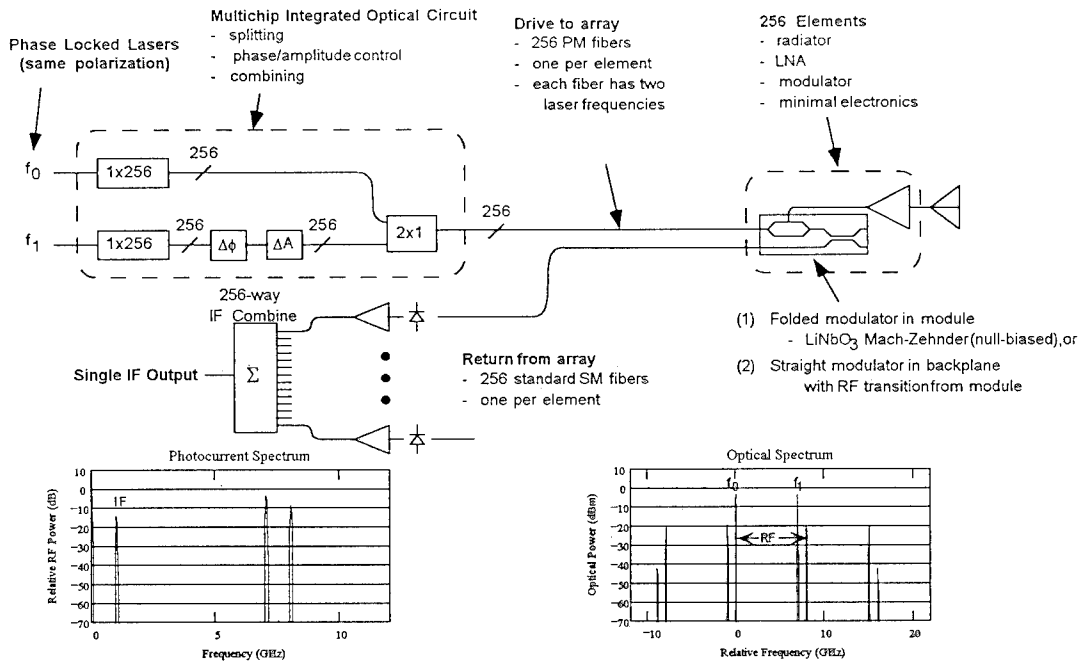


Figure 3.8.2-2. Receive Antenna Using Optical Downconversion

### 3.9 TECHNIQUES FOR FORMING MULTIPLE BEAMS

#### 3.9.1 Transmit Antenna

Figure 3.9.1-1 shows an architecture that can generate four independently controllable RF transmit beams. Much of the integrated optical circuit is repeated four times relative to the single beam controller. Optical carriers  $f_0$  and  $f_1$  are locked and input to the controller in separate waveguides. The  $f_1$  carrier is split four ways and modulated with the four IF information signals. The modulators could be phase or intensity modulators as discussed in previous sections. The modulated  $f_1$  carriers are further split, phase shifted, and attenuated as required to set the necessary complex weights for the four RF beams. The four  $f_1$  carriers are recombined with each other and then with the  $f_0$  carrier. Note that optical interference will occur between the residual  $f_1$  carriers. This has no impact on the antenna performance, since only the +1 modulation sidebands are used to carry the signals. The combined optical signals are photodetected, filtered, amplified, and radiated. The amplification must be linear because four signals are present.



- Using null-biased Mach-Zehnder
  - cleaner optical spectrum
  - same efficiency as phase modulator
  - bias control needed

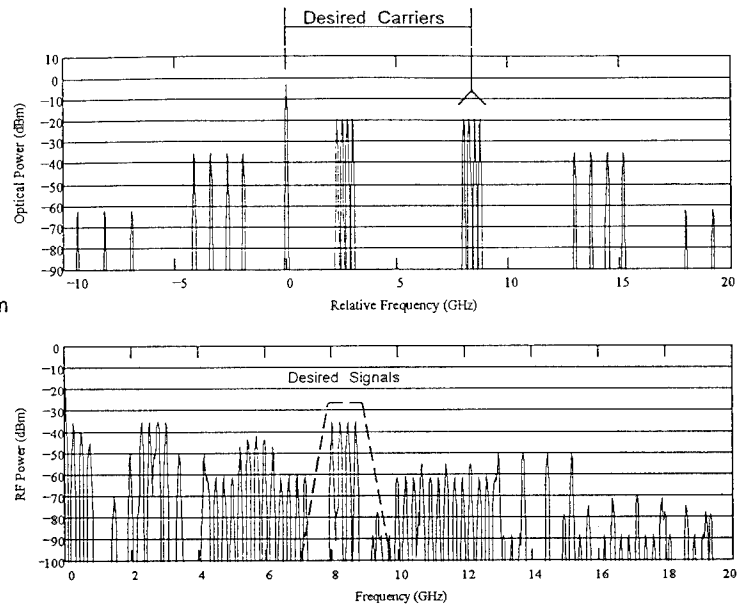


Figure 3.9.1-2. Optical and Photocurrent Spectra Using a Null-Biased Mach Zehnder

Figure 3.9-1.3 shows another example. For this case, an IF phase modulator was used. The phase modulator has exactly the same efficiency as the null-biased Mach-Zehnder modulator and does not require a bias controller. However, more spurs are generated. This is still not a problem for the present DSCS application.

- Using phase modulator
  - same efficiency
  - no bias control
  - more spurs

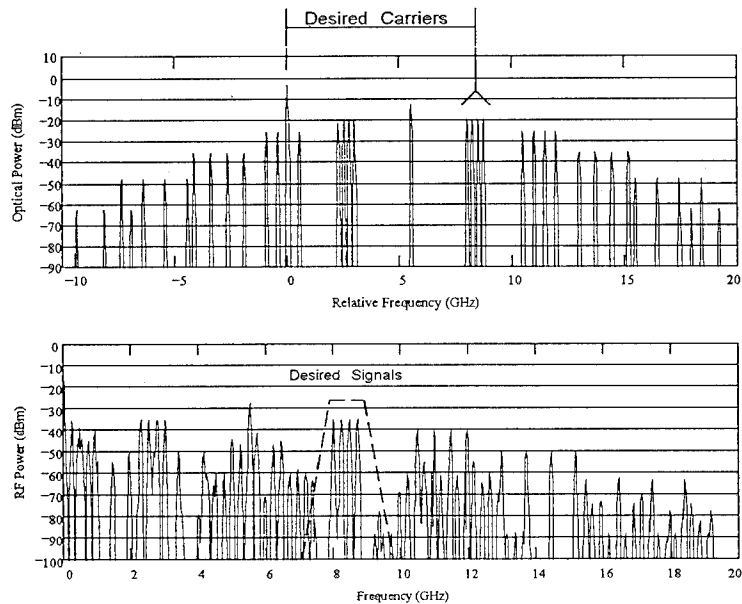


Figure 3.9.1-3. Optical and Photocurrent Spectra Using a Phase Modulator

### 3.9.2 Receive Antenna

Figure 3.9.2-1 shows a multiple beam receive architecture suitable for the DSCS application. For a 256-element array, 1024 phase controls are required. The integrated optical controller has four times the complexity of the previously discussed single beam case. This architecture uses electronic downconversion. The received signal is amplified and split four ways. Four electronic mixers are used to generate four separate IF signals. The four local oscillator signals are obtained from four photodiode and four optical fibers. The number of fibers could be reduced with some type of wavelength division multiplexing, but we expect that is not practical. The four IF signals from each antenna module are sorted and combined with the signals from the other elements to form the four beams. The combined signals can be returned to the array processor on IF fiber optic links, if desired.

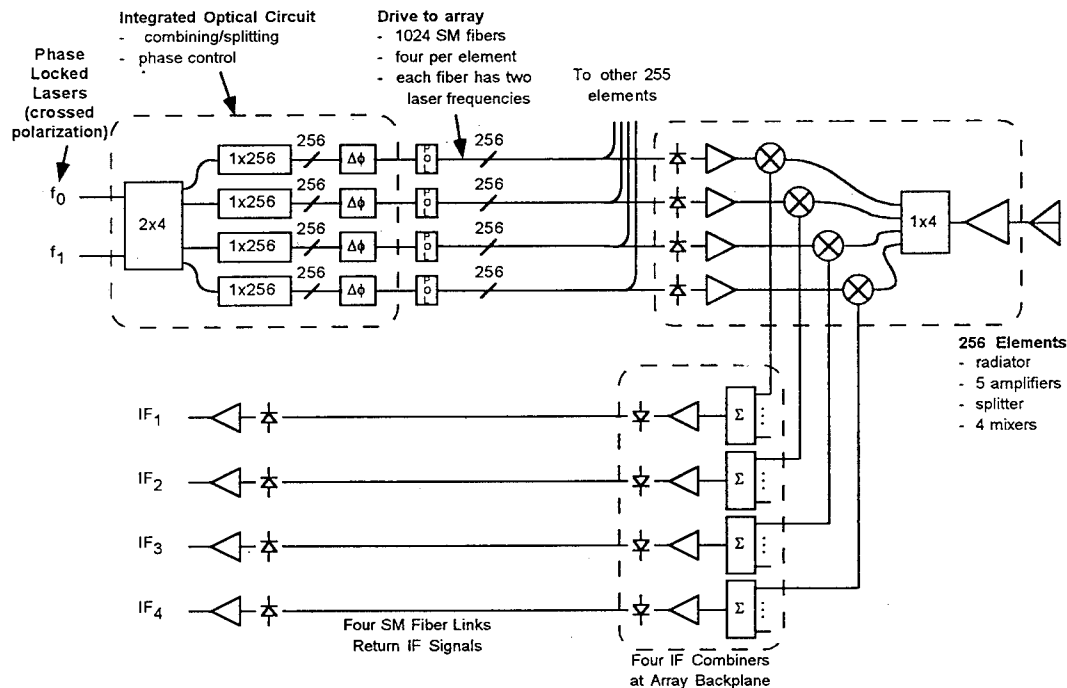


Figure 3.9.2-1. Multiple Beam Receive Antenna With Electronic Downconversion

An approach using optical downconversion is shown in Figure 3.9.2-2. This technique uses a common reference optical carrier  $f_0$ . Each of the RF beams uses a separate phase and amplitude controlled carrier  $f_1$ ,  $f_2$ ,  $f_3$ , and  $f_4$ . These four carriers are all phase locked to the  $f_0$  carrier, but with offsets that will mix the four receive signals down to non-overlapping IF bands. The advantage of this approach is that the antenna module only requires one modulator to perform all four downconversions simultaneously. The disadvantages are that putting an optical modulator in the antenna module is more complex than putting electronic mixers in the module. Also, if the modulator is polarization sensitive, polarization maintaining optical fiber is required between the integrated optical controller and the elements.

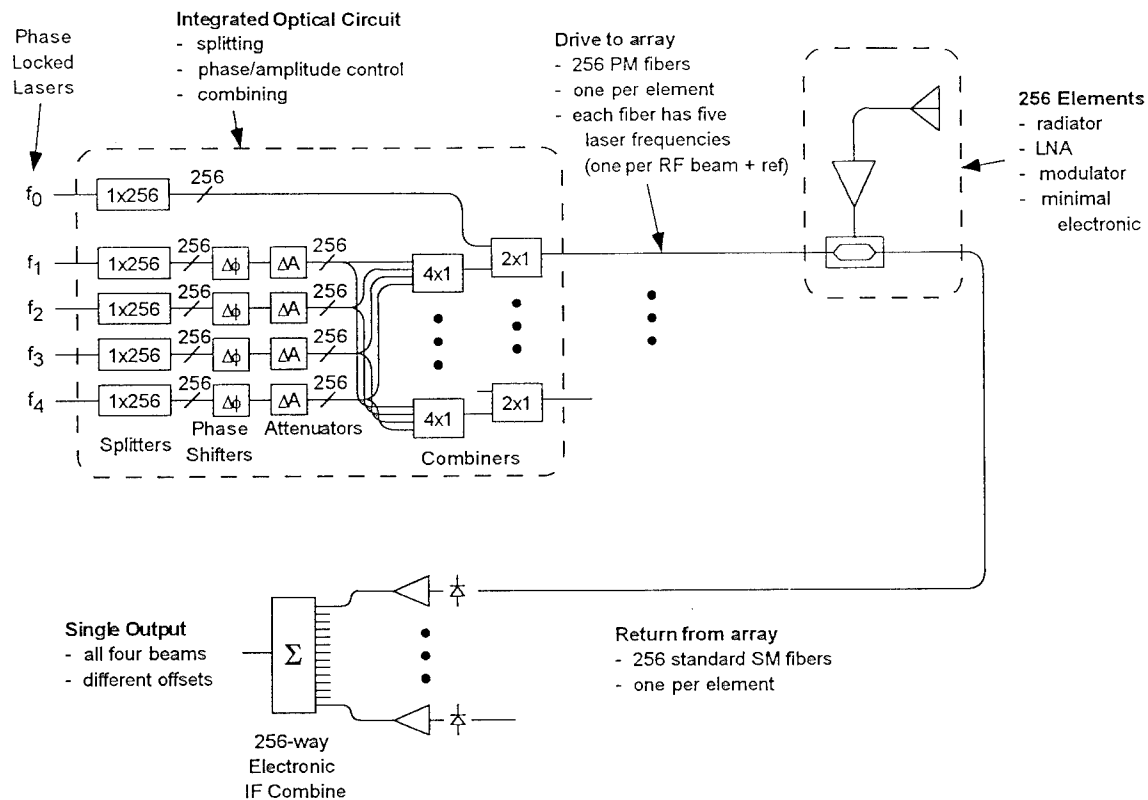


Figure 3.9.2-2 Multiple Beam Receive Antenna With Optical Downconversion

### 3.10 JAMMER NULLING

The space-based receive antenna requires the capability to form three simultaneous broadband (500 MHz wide) nulls in the antenna pattern in order to reduce the impact of jammers on the uplink. This capability forces tighter specifications on many system parameters. For example, good channel-to-channel tracking between individual elements in the phased array increases in importance. For a 40 dB deep null, tracking of better than 0.1 dB in amplitude and  $0.5^\circ$  in phase is necessary over the entire RF band (ref. 1). All of the phase and amplitude controllers must have very fine resolution. Since it cannot be assumed that the jammers all come from the same direction, true time delay cannot be used to advantage. This is because zero time dispersion can only be set in a single direction. If the zero time dispersion direction is set to the main beam direction, the pattern nulls in the jammer directions will move with frequency (i.e., the nulls will be narrow band). Thus, true time delay doesn't help unless all of the jammers are in virtually the same direction as the main beam. We assume that a multiple sidelobe canceling scheme using phase and amplitude control will be implemented. Each jammer will require multiple auxiliaries so that there are enough degrees of freedom to form several broadband nulls. The number of auxiliaries needed to cancel a jammer depends on the depth of the null, the jammer's fractional bandwidth, its location relative to the main beam, and the size and amplitude taper of the receive array.

The critical parameter for analyzing broadband null depth is referred to as fractional dispersion (ref. 2). Fractional dispersion,  $M$ , is the product of the fractional bandwidth of the jammer and the number of beamwidths the jammer is located from the main beam. Assume that the space-based receive array has a filter that limits the receive bandwidth to 500 MHz. Also, assume that the signal paths are trimmed to equal length so that the zero time dispersion angle points broadside to the center of the earth. Then, the maximum fractional dispersion is  $M_{\max}=0.3$ , as shown in Figure 3.10-1.

Equation 3.158 from Mailloux (ref. 3) gives an estimate of the expected depth of a broadband null,  $D$ , as a function of  $M$ , the fractional dispersion, and  $N$ , the number of nulls (degrees of freedom). The equation is repeated here:

$$D = \left\{ \left( \frac{e}{2} \right)^{[1-(M/N)^2]} \frac{M}{N} \right\}^{2N},$$

where  $e$  is the base of the natural logarithm.

Figure 3.10-2 shows this result for various values of  $N$ . Note that the null depth is relative to the envelope of the quiescent sidelobe pattern. Thus, the total jammer rejection is the sum of the rejection due to the amplitude tapering of the array plus the reduction due to the sidelobe cancelers. The dots in Figure 3.10-1 show that a single null (one degree of freedom) is expected to give only about an 8 dB improvement relative to the sidelobe envelope. Two nulls (two degrees of freedom) yield about a 28 dB null over the entire 500 MHz jammer bandwidth.



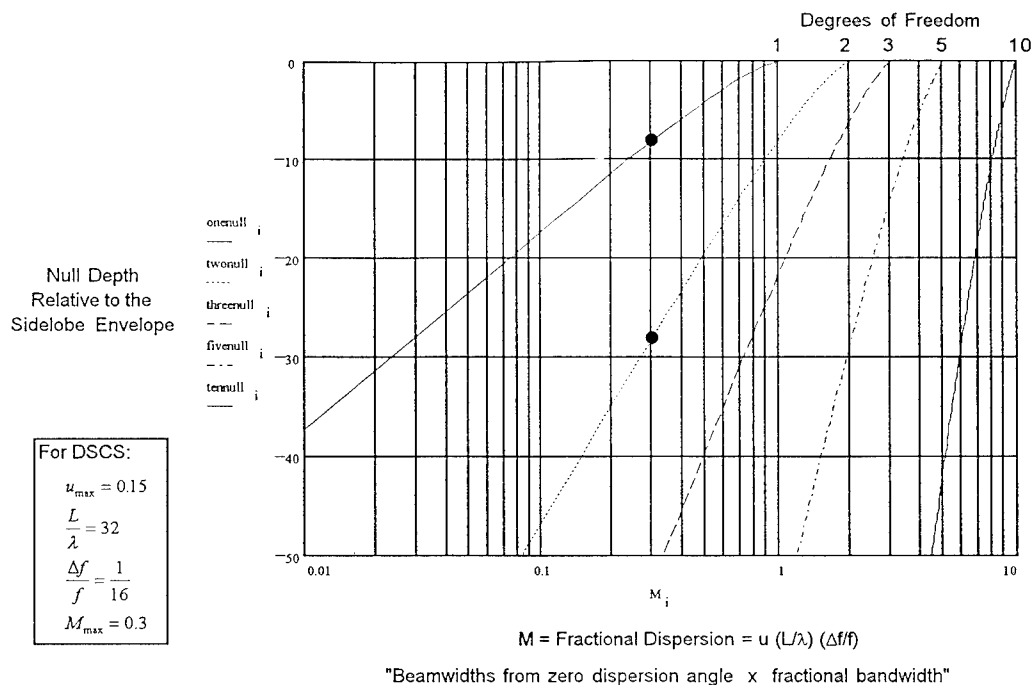
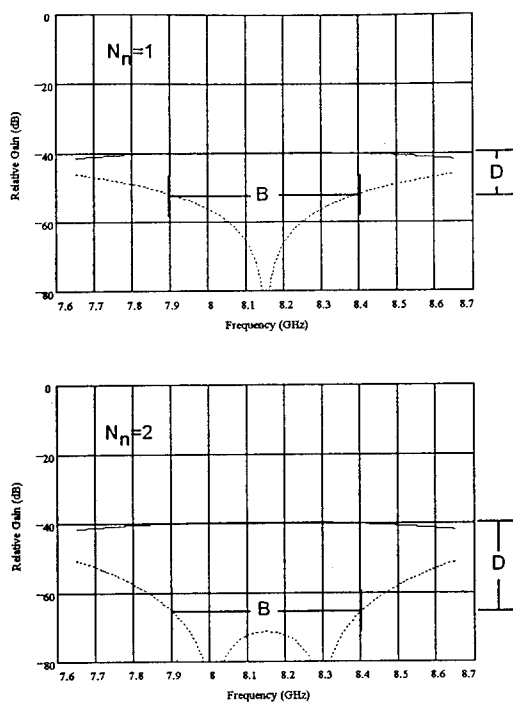


Figure 3.10-1. Null Depth Versus Fractional Bandwidth and Degrees of Freedom

An graphical illustration of what is occurring is shown in Figure 3.10-2. The solid lines show the antenna gain before adaptation. The dashed lines are after adaptation. With a single degree of freedom, as shown in the top half of the figure, the null is sharp and not very deep over a broad bandwidth ( $B=500$  MHz). The bottom half of the figure shows that two degrees of freedom allow the null to be pulled significantly deeper over the entire bandwidth. The separation between the two zeros is optimized depending on the bandwidth of the jammer. With one or two degrees of freedom, the jammer rejection relative to the sidelobe envelope is about 12 dB or 25 dB, respectively. The null can be further broadened and deepened with still more degrees of freedom.



Null depth,  $D$ , is a function of:

- jammer direction,  $\theta_0$
- jammer bandwidth,  $B$
- array length,  $L$
- number of adapted nulls,  $N_n$

$$D \cong \left\{ \left( \frac{e}{2} \right)^{1 + \left( \frac{M}{N_n} \right)^2} \cdot \frac{M}{N_n} \right\}^{2N_n}$$

$$M = \sin \theta_0 \cdot \frac{L}{\lambda_0} \cdot \frac{B}{f_0}$$

Null bandwidth can also be limited by frequency tracking errors between elements

Figure 3.10-2. Null Depth Versus Number of Nulls (Degrees of Freedom)

Figure 3.10-3 shows the proposed layout for the space-based receive array. For this discussion, it is assumed that the 253 elements are laid out on a triangular grid in a circular aperture with  $2\lambda$  spacing. This results in an array that is slightly larger than one square meter in area. The circles indicate the six elements that are used to adapt to jammers. The choice of elements was not optimized. These six were selected based on the assumption the array will eventually be implemented with an amplitude taper. In that case, the outer elements will be intentionally attenuated to reduce the sidelobes. The use of these elements for jammer canceling will, therefore, have minimal impact on the main beam and will make use of signal power that would otherwise have been discarded.

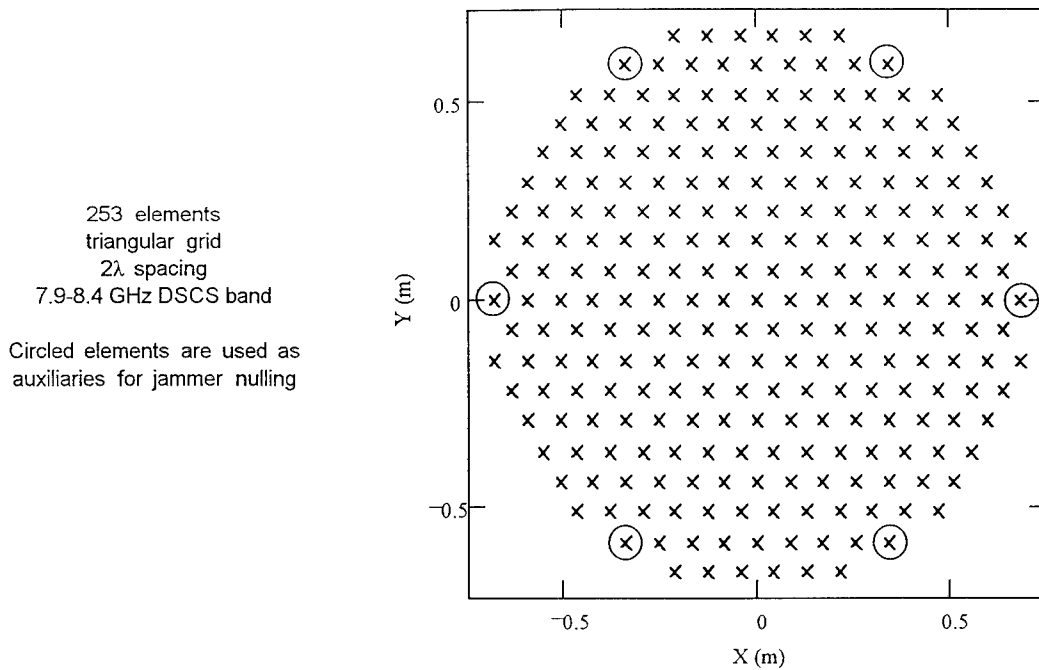


Figure 3.10-3. Array Configuration Used For Jammer Nulling Examples

Figure 3.10-4 shows the array factor for the antenna when all 253 elements are uniformly weighted. As expected, the pattern looks like the diffraction pattern from a circular aperture. The plot uses the conventional  $(u,v)$  direction cosine coordinate system as defined in the figure, where  $\theta$  is the angle from broadside, and  $\phi$  is the angle of rotation from the  $x$ -axis toward the  $y$ -axis. The circle represents the mapping into the  $(u,v)$  space of the  $17.34^\circ$  wide earth as viewed from geosynchronous orbit.

White areas indicate maximum gain  
Dark areas indicate minimum gain  
(5 dB per contour)

Direction cosines:

$$u = \sin \theta \cos \phi$$

$$v = \sin \theta \sin \phi$$

The circle shows the 17.34° angle  
subtended by the earth  
from geosynch orbit

$$\sqrt{u^2 + v^2} = \sin\left(\frac{17.34^\circ}{2}\right) = 0.15$$

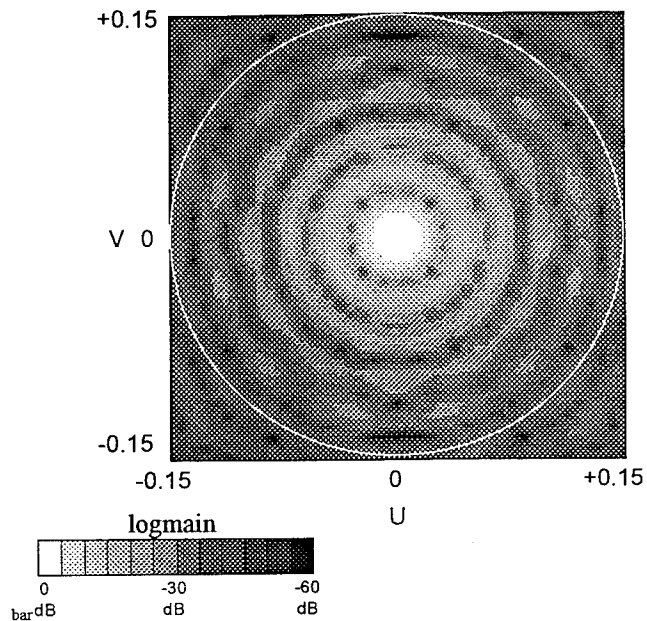


Figure 3.10-4. Array Factor With Uniform Weighting

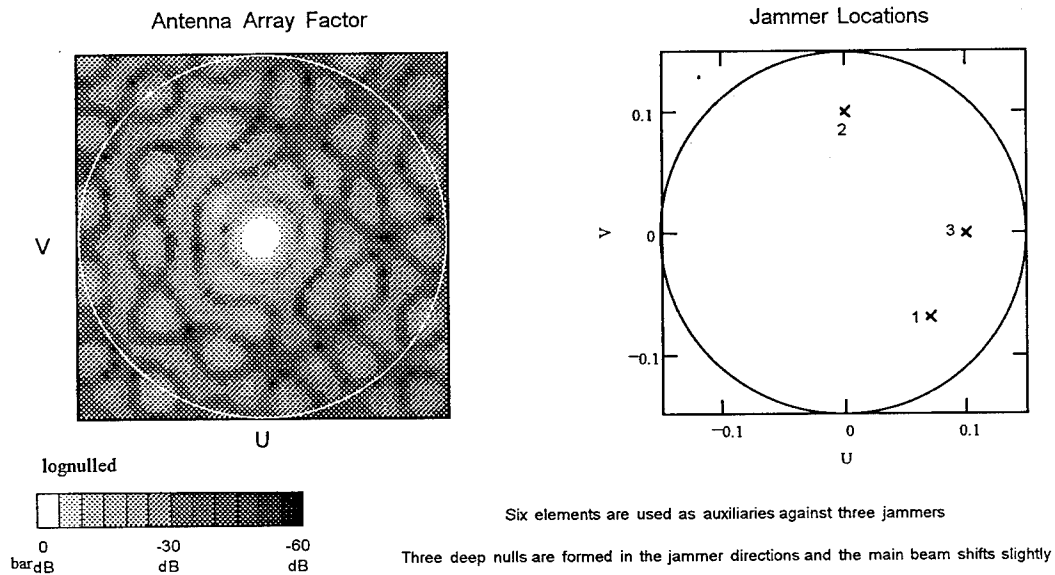


Figure 3.10-5. Jammer Nulling Example (3 Jammers and 6 Degrees of Freedom)

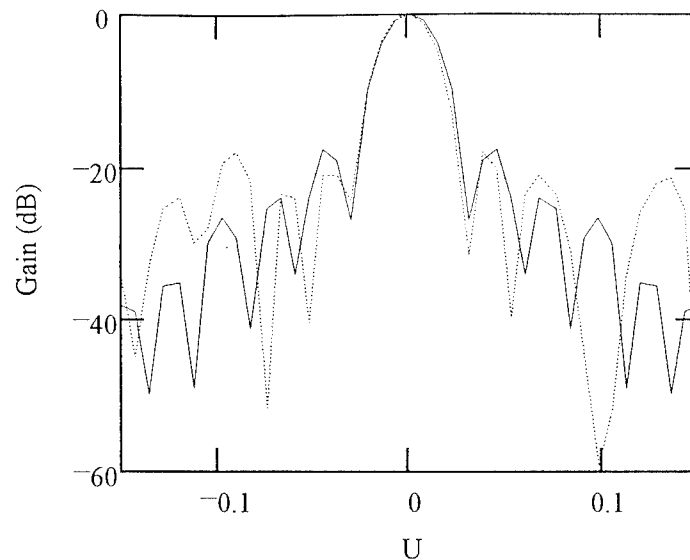


Figure 3.10-6. Array Pattern Along the  $V=0$  axis Before (solid) and After (dashed) Adaptation.

An analysis was performed following the analysis of White (ref. 2) that computes the optimal adapted weights using a Howells-Applebaum approach. Figure 3.10-5 shows the resulting antenna pattern when three jammers are present. The angular positions of the jammers are also shown in the right half of the figure. The jammers are located near the maximum of the third sidelobe ring. The sidelobe pattern rearranges to place deep nulls in the jammer directions. The main beam is not significantly perturbed.

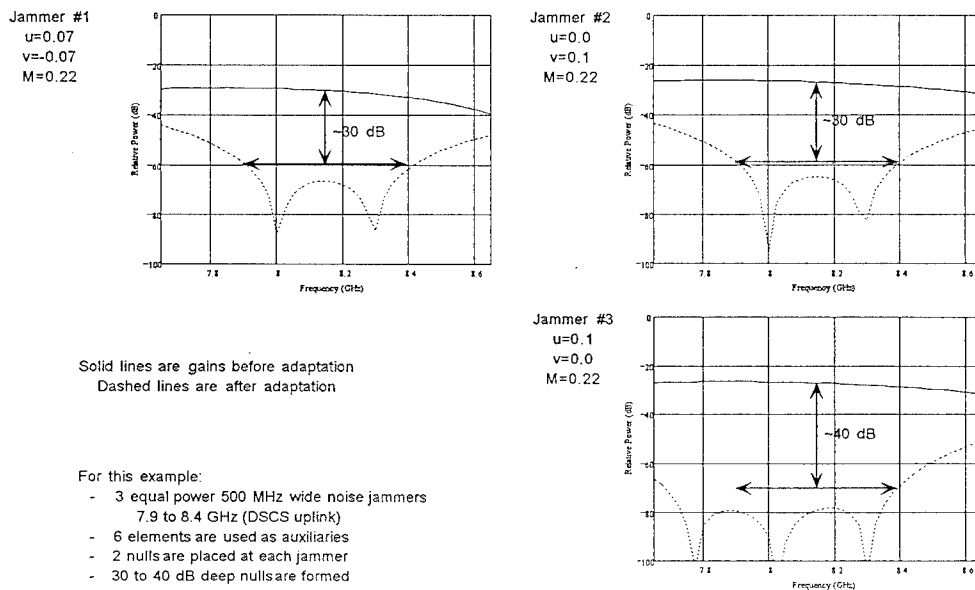


Figure 3.10-7. Null Bandwidths

Figure 3.10-6 shows the frequency response of the adapted array in each of the jammer directions. The jammers were assumed to be 500 MHz wide noise jammers. The adapted nulls are approximately 30, 30, and 40 dB deep relative to the quiescent sidelobe envelope. Referring to Figure 3.10-1, null depths of about 35 dB are expected with  $N=2$  (per jammer) and  $M$  of 0.22.

The conclusion of this analysis is that, for the space-based receive application, six adaptable elements are probably sufficient to null three jammers. The nulls formed are about 35 dB deep relative to the sidelobe envelope. In practice, amplitude and phase inaccuracies are expected to limit forcing the nulls any deeper. The effects of amplitude and phase errors are further discussed in the next section.

Amplitude tapers can be used to further reduce the sidelobe envelope relative to the uniformly-weighted circular array used in the preceding example. Figure 3.10-7 shows the antenna pattern using a 40 dB circular Taylor weighting. The sidelobe envelope is now 40 dB down from the main beam peak. Adaptive jammer nulling will further attenuate unwanted signals by placing nulls as shown in Figure 3.10-8.

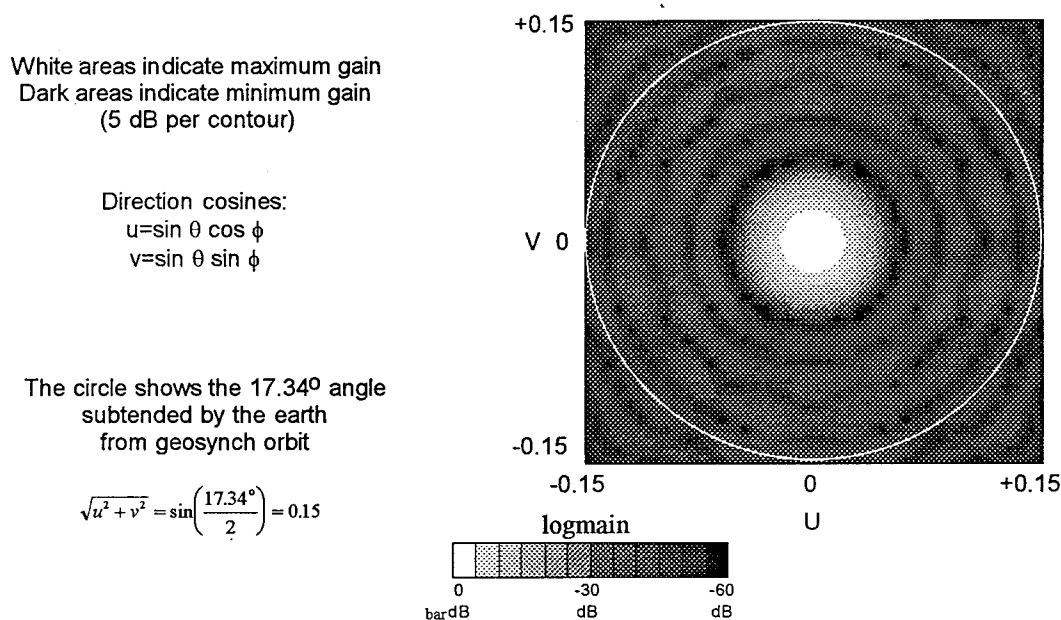


Figure 3.10-8. Antenna Pattern with 40 dB Taylor Weighting and No Jammers

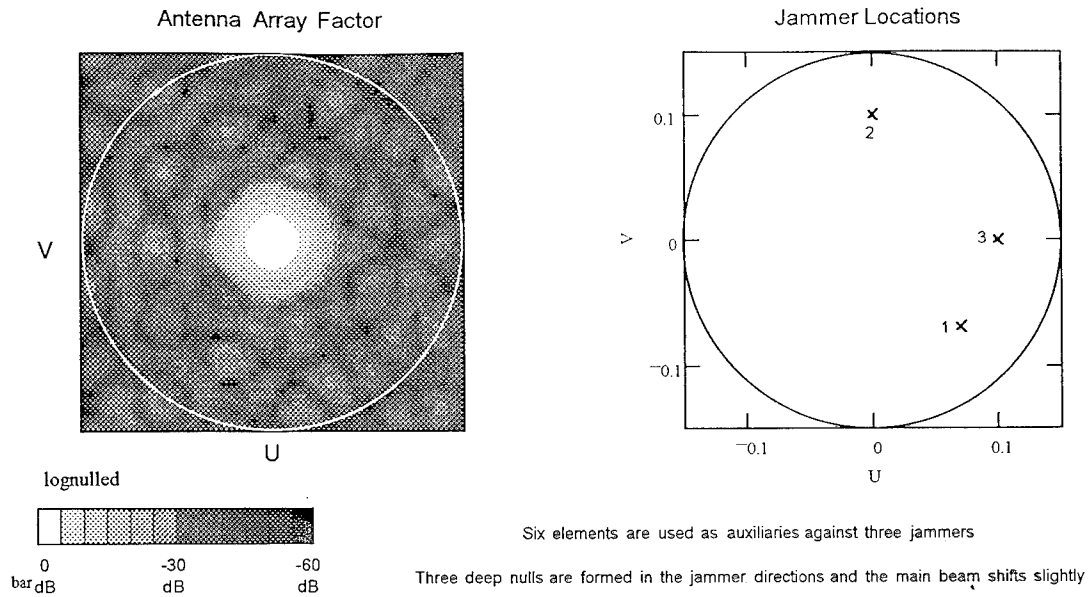


Figure 3.10-9. Adapted Pattern With Taylor 40 dB Weighting and Three Jammers

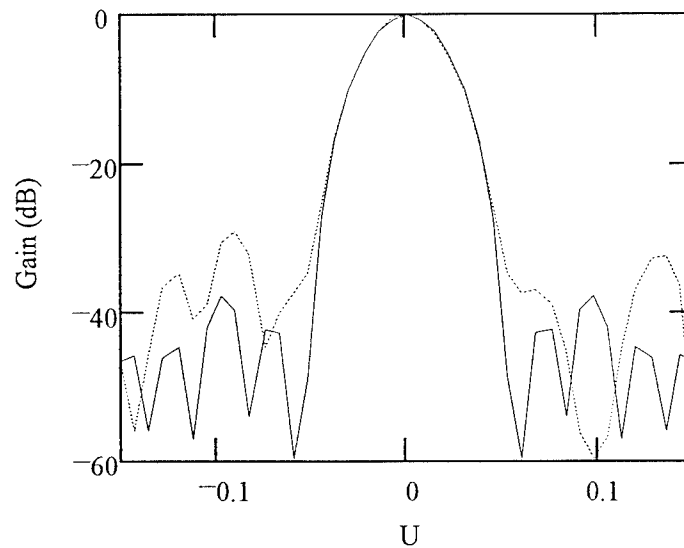


Figure 3.10-10. Array Pattern Along the  $V=0$  axis Before (solid) and After (dashed) Adaptation.

### 3.11 IMPACT OF PHASE AND AMPLITUDE ERRORS

The previous section described the techniques for jammer nulling with no consideration for phase and amplitude errors on the individual antenna elements. In this section, the limitations imposed by errors are discussed. A 16-element linear array is used as an example to simplify the discussion.

Figure 3.11-1 shows data for a 16-element linear phased array with  $2\lambda$  spacing. This is similar to a one-dimensional cross-section of the space-based SHF array. Figure 3.11-1 shows the case of no amplitude taper, with all of the elements in phase. The antenna pattern has the usual  $\sin(Nx)/N\sin(x)$  form. We define a gain factor and beam broadening factor as shown in the figure. Both quantities are normalized to unity for the uniform amplitude weighting case.

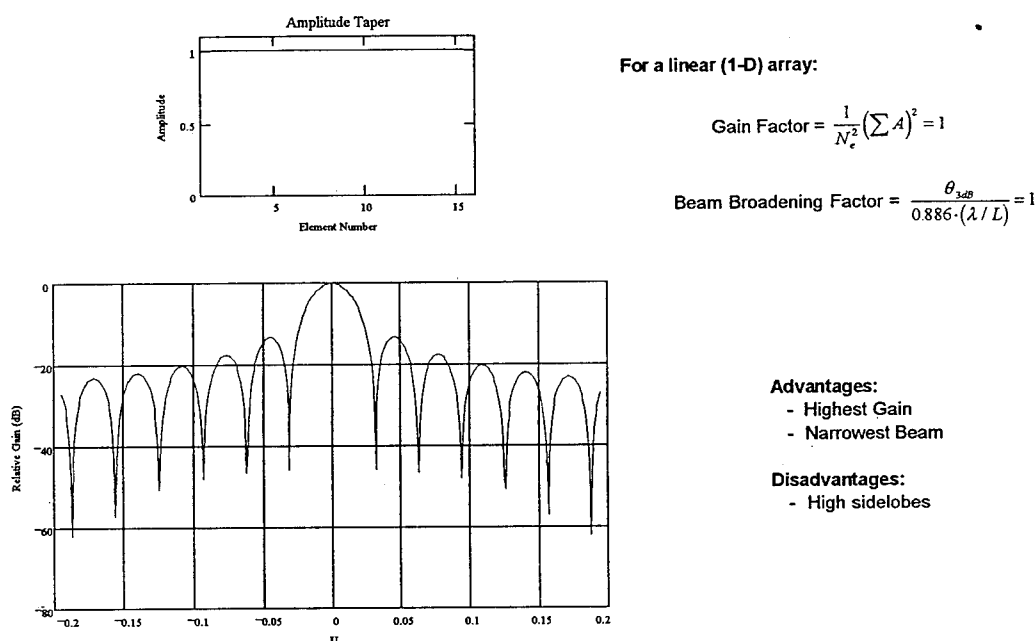


Figure 3.11-1. Array Factor With Uniform Weighting

Figure 3.11-2 shows an example of a Taylor amplitude weighting with 40 dB sidelobes and  $\bar{n}=5$  (ref. 3). The sidelobes are significantly lower than for the uniformly weighted case. This increases the rejection of jammers coming from directions other than the main beam. The disadvantages are that the main beam gain of the array is reduced by about 5 dB, and that the main beam is broadened by about 40%. The loss in gain implies a loss in signal to noise ratio out of the receiver. The broader main beam means that more jammers will now fall in the main beam, where rejection is much more difficult. The choice of amplitude taper is a trade that requires more information on the jammer environment to determine. For the purposes of this discussion, the use of a Taylor window highlights the impact of phase and amplitude errors.



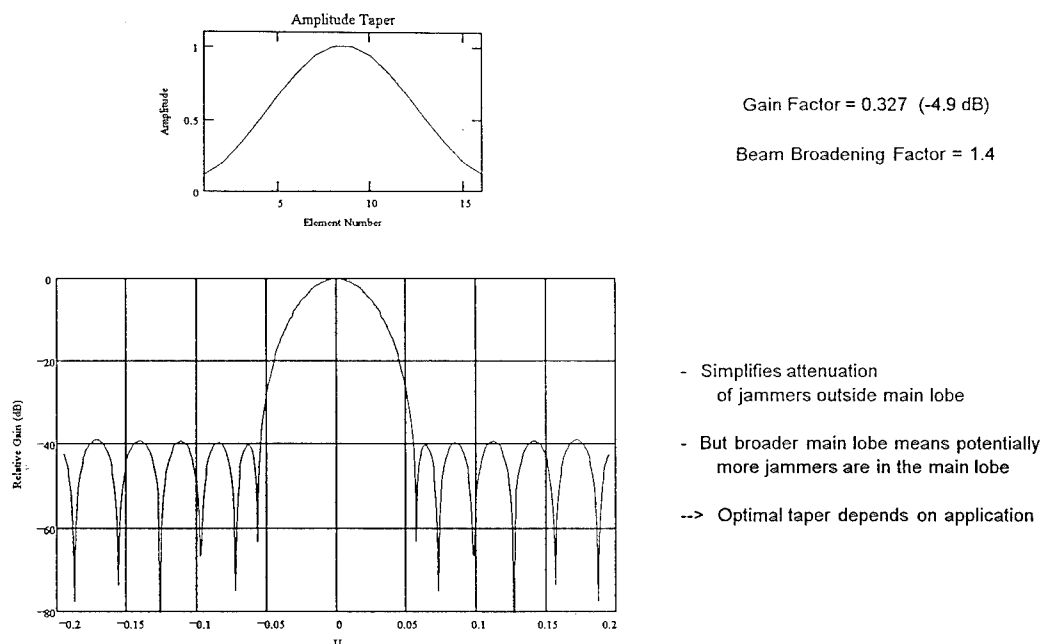
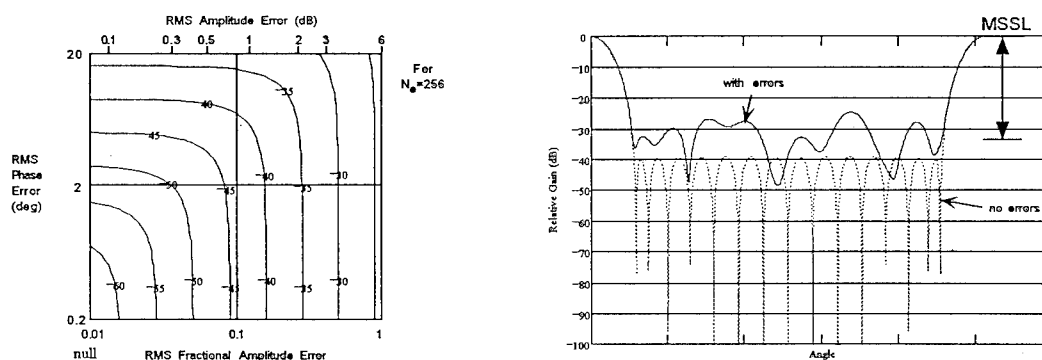


Figure 3.11-2. Array Factor With Taylor Weighting (40 dB,  $\bar{n} = 5$ )



Mean-square side lobe (MSSL):

$$MSSL \cong \frac{\sigma_A^2 + \sigma_\phi^2}{N_e}$$

$\sigma_A$  = RMS fractional amplitude error

$\sigma_\phi$  = RMS phase error (rad)

$N_e$  = Number of elements

Example:

16 elements

40 dB Taylor window

Each element has  $5^\circ$  RMS random phase error

No amplitude errors

MSSL = -33 dB

Figure 3.11-3. Effect of Amplitude and Phase Errors on Sidelobes

Figure 3.11-3 shows what happens to the array pattern when phase or amplitude errors are added to the elements. The errors cause a mean-square sidelobe level (MSSL) that adds to the ideal sidelobes resulting

from the amplitude taper. For the example shown, a  $5^\circ$  RMS phase error on each element leads to a MSSL of -33 dB relative to the main beam peak. Because of the random nature of the errors, some sidelobes are higher and some are lower than the mean.

The contour plot on the left side of the figure is drawn for the SHF array application which has 256 elements. In order to achieve a MSSL of -40 dB, the RMS phase error must be less than about  $10^\circ$  and the RMS amplitude error must be less than about 1 dB.

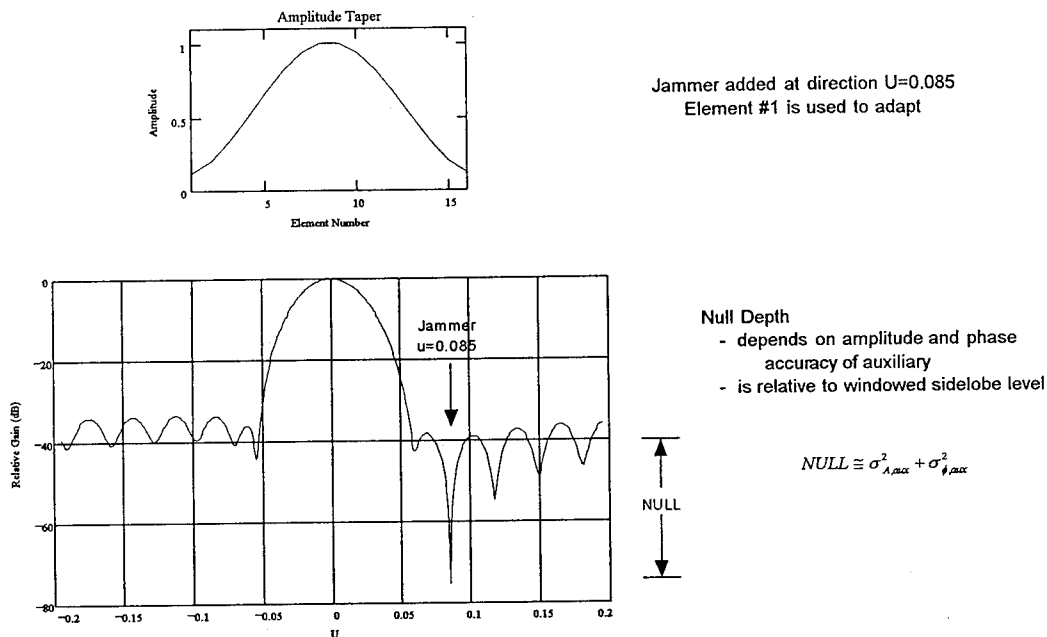


Figure 3.11-4. Array Pattern With a Single Adapted Null

When an auxiliary is used to adapt to a jammer, a deep null can be formed as shown in Figure 3.11-4. The auxiliary can be another antenna separate from the main array, or it can be one of the main array elements as shown in our example. The expected depth of the null at a single frequency depends again on the accuracy with which the auxiliary amplitude and phase can be adjusted. For this case, however, the depth of the null is with respect to the sidelobe level of the amplitude-tapered array in the direction of the jammer. Figure 3.11-5 shows a contour plot of the null depth relative to the sidelobe level for a single auxiliary.

For the case of the 256-element SHF phased array with RMS phase and amplitude errors of  $10^\circ$  and 1 dB, the resulting MSSL was about -40 dB. If we use one of these same elements to place an adaptive null in the direction of a jammer, the expected null would drop about 15 dB below the sidelobe level in the direction of the jammer. For the Taylor window, this would give an expected total jammer rejection of about 55 dB.

Using the Boeing electrooptical phase and amplitude controlling approach, the elements can have continuous analog control. Thus, a good jammer nulling architecture may use relatively coarse digital control of most of the array elements to set the main beam direction and amplitude taper. Then a few

elements used in a jammer-nulling feedback loop could have much finer control — either analog or digital.

In summary, the total amount of jammer rejection is approximately given by the sum of the mean sidelobe level in the direction of the jammer plus the additional depth of the null that can be formed. The exact numbers depend on amplitude tapering and individual element phase and amplitude accuracies.

Null depth relative to sidelobe level:

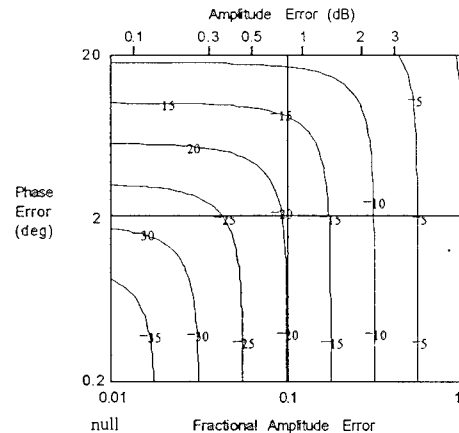
$$\text{Null Depth} \cong 10 \cdot \log \{ \sigma_A^2 + \sigma_\phi^2 \}$$

where:  $\sigma_A$  = fractional amplitude error

$\sigma_\phi$  = phase error (rad)

Errors can be due to:

- channel tracking
- phase / amplitude controller resolution



$$\text{Amplitude Error (dB)} = 20 \cdot \log(1 + A)$$

Figure 3.11-5. Null Depth Limit With Phase and Amplitude Errors

The discussion so far has been concerned only with jammer rejection in a single direction and at a single frequency. Another level of complexity occurs when the jammer has a nonzero bandwidth, such as for a broadband noise jammer. The previous section described the bandwidth of nulls generated with frequency-independent complex weights without phase and amplitude tracking errors. The results presented there were best case. With tracking errors, the null bandwidth is further degraded. For example, assume that the complex weights are chosen to create a perfect null at some frequency  $f_0$ . Assume also that the element tracking errors are such that at  $f_0 + \Delta f$  the elements have random phase and amplitude deviations of  $\sigma_\phi$  and  $\sigma_A$ . Note that the deviation is from the actual phases and amplitudes of the elements at  $f_0$ , not from the ideal phases and amplitudes. Then, the expected depth of the null is limited by the MSSL given by

$$MSSL = \frac{\sigma_\phi^2 + \sigma_A^2}{N_e}$$

### 3.12 CHOICE OF OPTICAL WAVELENGTH

A trade study was conducted to look at the cost of optical power at various wavelengths. Lasers operating at 830, 985, 1300, and 1550 nm were considered. The results are shown in Figure 3.12-1. The antennas under consideration for this contract require on the order of a few watts of optical power. The table shows that high power semiconductor lasers at 985 and 830 nm give the minimum cost per milliwatt of optical power. Nd:YAG lasers operating at 1319 nm are the next in line. Prices on all of these components are dropping while output powers are increasing. Discussions with vendors indicate that the lowest cost solution may soon be semiconductor amplifiers at 1300 or 1550 nm or erbium-doped fiber amplifiers at 1550 nm. The push is clearly toward higher power devices and longer wavelengths.

Single Line Laser Sources (1995 Data)				Isolated SMF- Coupled				
Wavelength (nm)	Single- Line Laser Type	Example Manufacturer	Cost (k\$)	Add'l Isolator (-1dB) (k\$)	Add'l Pigtail (-1 dB) (k\$)	Output Power (mW)	Bucks for the Bang (\$/mW)	Bang for the Buck (mW/k\$)
830	FP	SDL-5430	2.2	1	1	120	35	28.6
985	MOPA	SDL-5762 +	9.7	1	1	600	20	51.3
1300	DFB	Ortel	10			16	625	1.6
		Fujitsu	5			20	250	4.0
	YAG	Lghtwv Electr.	30	1	1	300	107	9.4
		Micracor	15			100	150	6.7
1550	DFB	UTP	7.3			20	365	2.7

Figure 3.12-1. Cost Comparison of Various Laser Sources

### 3.13 PROOF OF CONCEPT DEMONSTRATION

A four-element optically controlled phased array was set up and demonstrated at Boeing before the present contract began. This apparatus was demonstrated to representatives from Rome Laboratory during an oral contract review at Boeing in order to satisfy the contract requirement for a proof of concept demonstration. The demonstration to Rome Laboratory was operating at 18 GHz in a four-element receive configuration. Boeing has demonstrated with this apparatus center frequency operation from 18 to 40 GHz in both transmit and receive. The following photographs and experimental results are for a transmit array operating at 20 GHz.

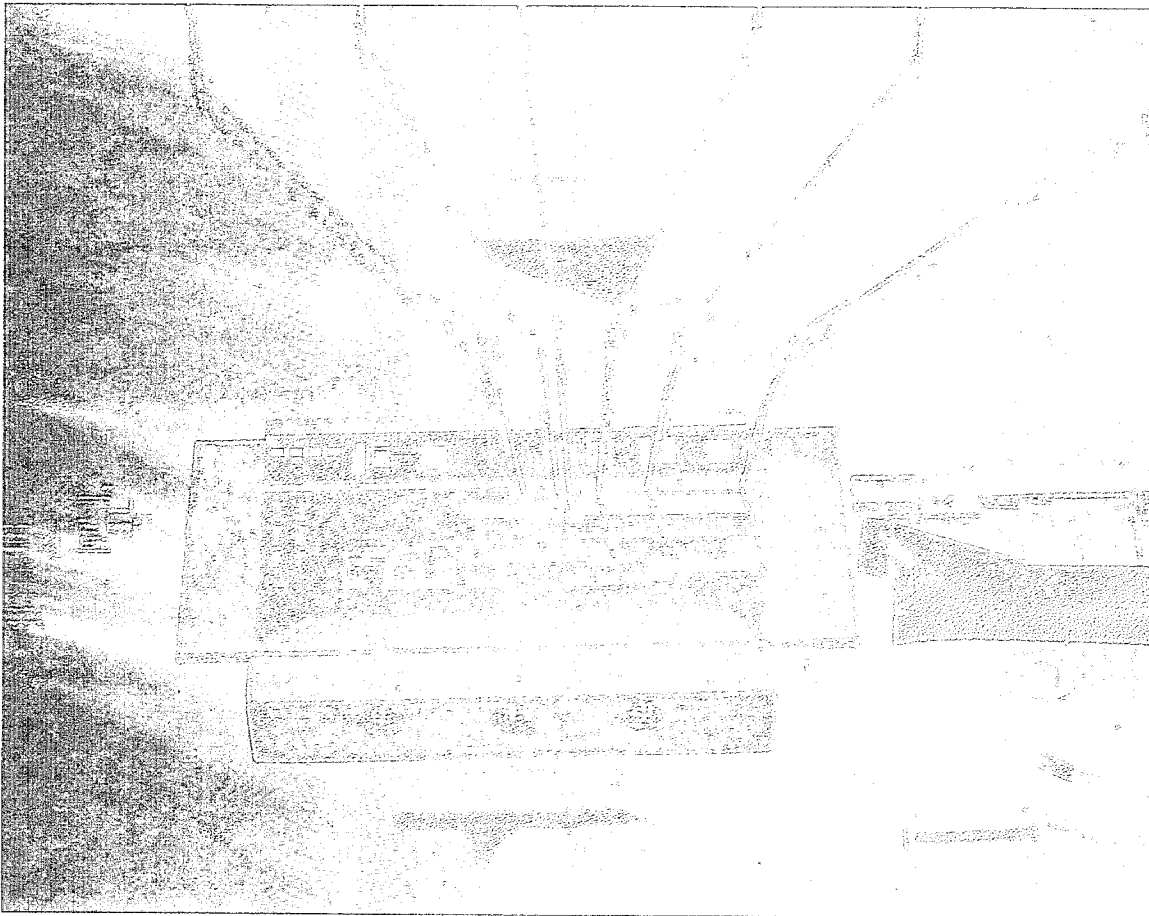


Figure 3.13-1. Four-Channel Phase Controller Integrated Optical Circuit

Figure 3.13-1 shows the four-channel integrated optical phase controller circuit. The device used in the demonstration was not packaged. The input fiber on the left side of the diagram contains power from two diode-pumped Nd:YAG lasers with a frequency separation of 20 GHz. The single input contains both frequencies in orthogonal polarizations. The integrated optical controller splits the input power four ways. Five electrodes are used. The control voltages were applied through six DC probes as shown (five voltages and ground). The first four electrodes give individual phase control for each element. The fifth electrode is arranged so that a single voltage can apply a linear phase tilt across all four elements. This linear phase tilt

steers the RF transmit beam. The first four electrodes are used to adjust the element phases to form a broadside beam with the common steering electrode set at 0 volts. At the right edge of the figure is the four-fiber output.

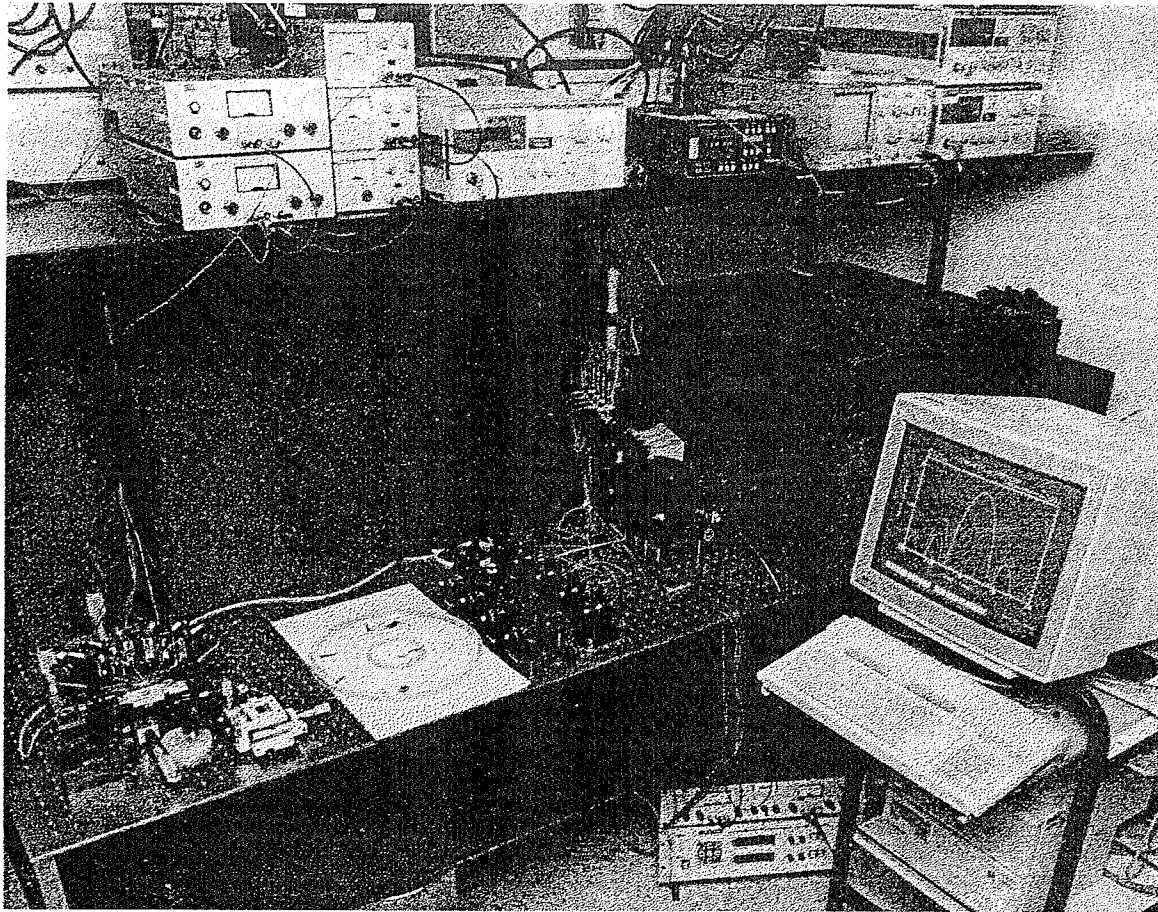


Figure 3.13-2. Optically Controlled Phased Array Test Apparatus

Figure 3.13-2 shows the laboratory apparatus. The integrated optical phase controller is located at the left edge of the photo. The four element array is in the center of the photo on a computer-controlled rotation stage. Each element consists of a photodiode, a bias-T, a microwave amplifier and a standard gain horn. Five power supplies are located on the shelf above the integrated optical circuit for adjusting the electrode voltages. A small anechoic chamber was constructed on the table using microwave absorbing material. The computer controller is in the lower right corner. A receive standard gain horn was located at the far end of the anechoic chamber. The received power was monitored while the 1x4 array was rotated in order to measure radiation patterns.

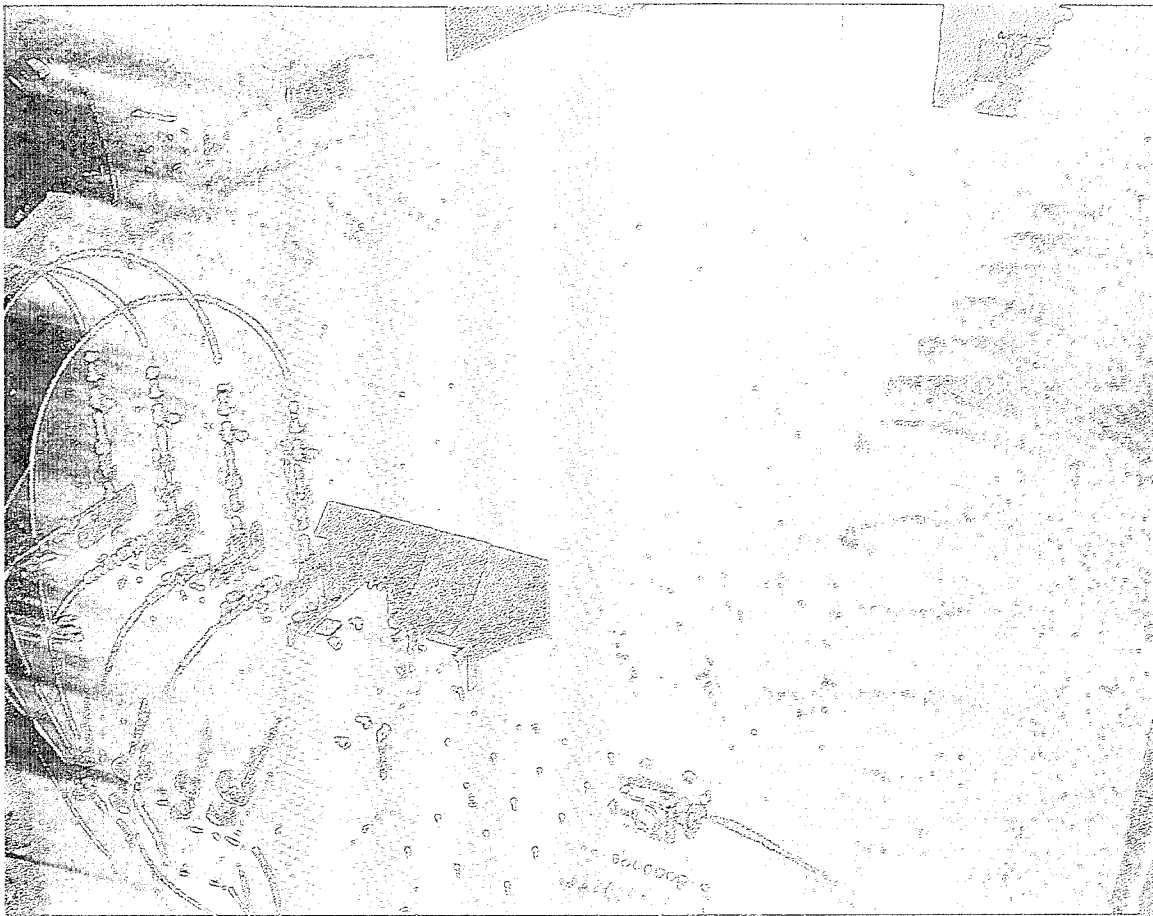


Figure 3.13-3. Miniature Anechoic Chamber (With Top Removed)

Figure 3.13-3 shows a close-up view of the anechoic chamber with the top removed. The 1x4 transmit array is in the lower left corner of the figure. The receive horn is located at the upper right corner. Figures 3.13-4, 5, and 6 show a sequence of antenna pattern measurements for various steering electrode voltages. The solid lines are the measured data. The dashed lines are the calculated patterns using the array factor and the standard gain horn element pattern. The four individual phase control electrodes were adjusted to form a broadside beam with 0 volts on the common steering electrode. These electrode voltages were not adjusted during the sequence of measurements. Figure 3.13-7 is a plot of the main beam angle versus steering electrode voltage. The beam angle is very linear with control voltage.

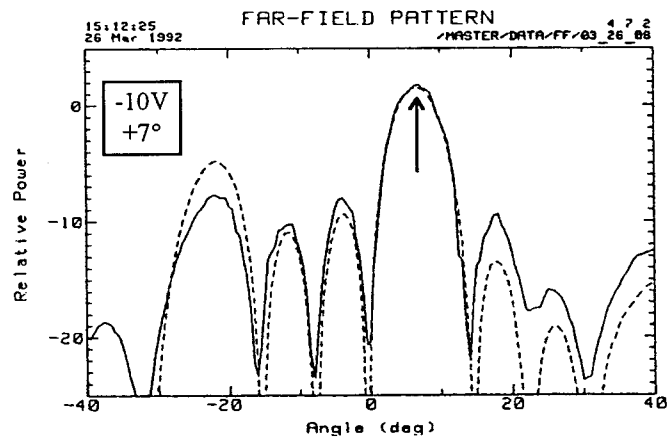
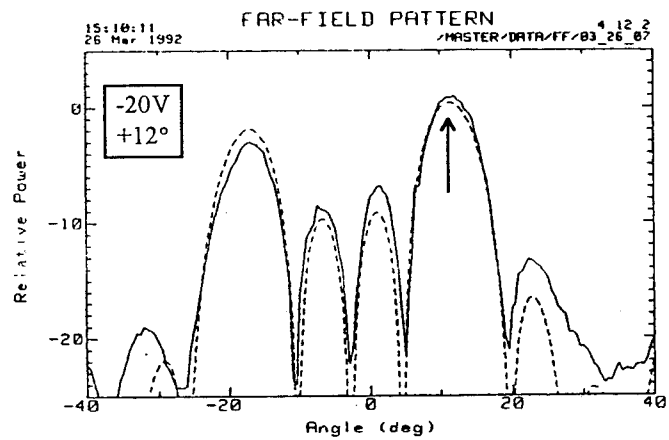
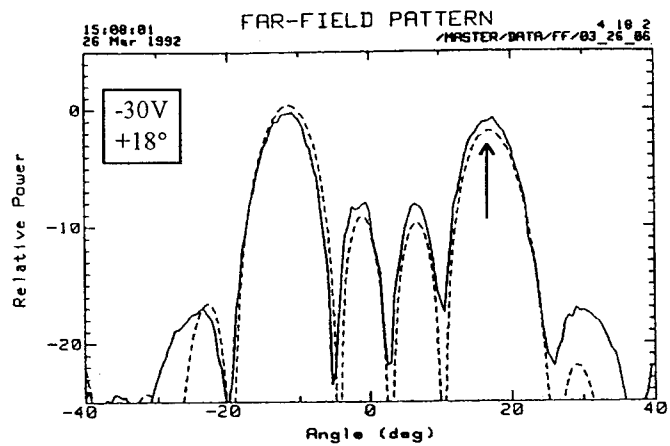


Figure 3.13-4. Antenna Patterns at -30 V, -20 V, and -10 V Steering Voltages



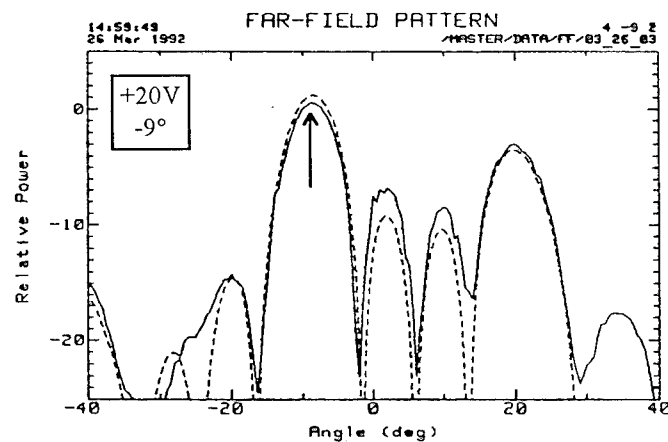
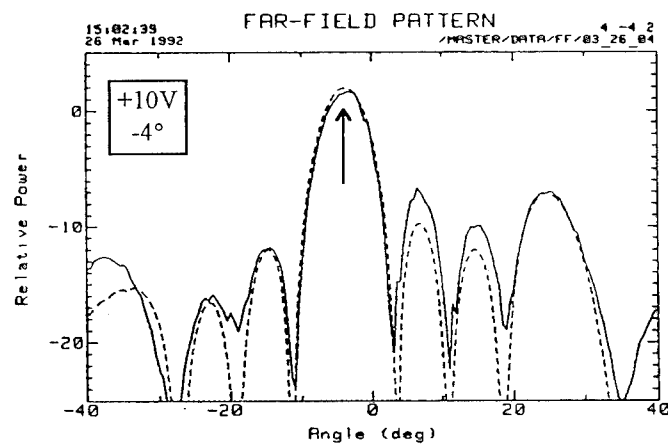
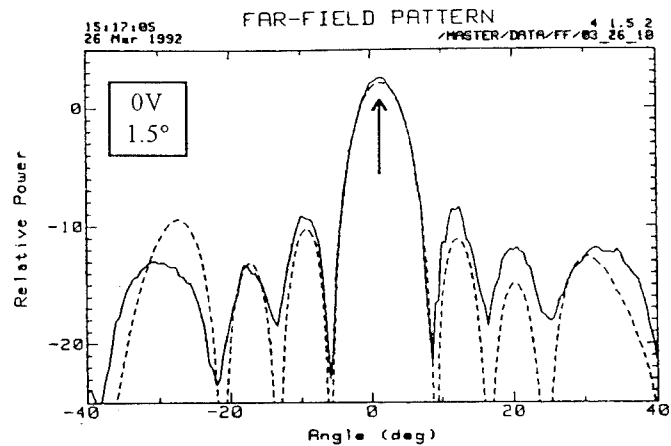


Figure 3.13-5. Antenna Patterns at 0 V, +10 V, and -20 V Steering Voltages

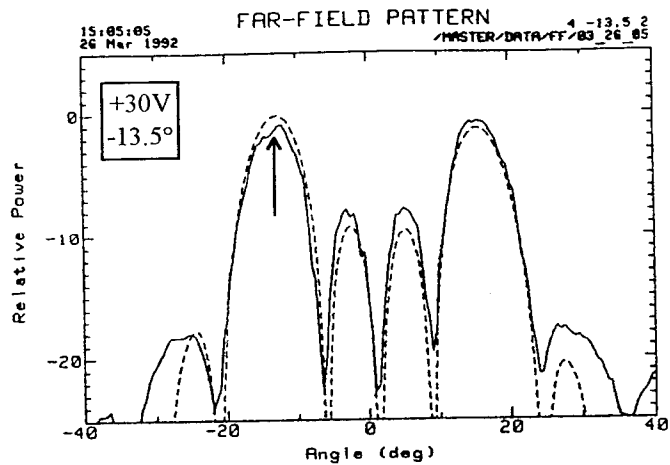


Figure 3.13-6. Antenna Pattern at +30 V Steering Voltage

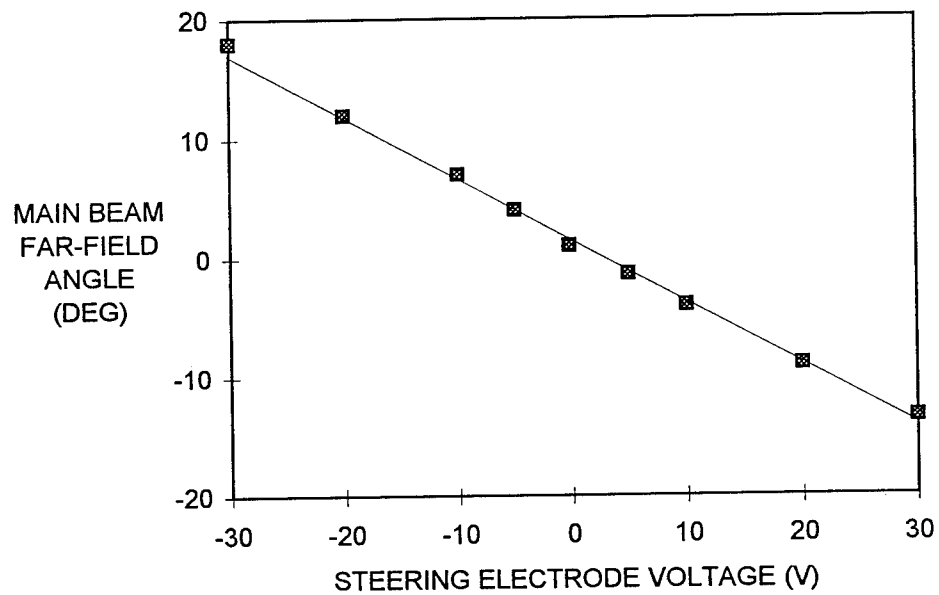


Figure 3.13-7. Linear Tuning of Main Beam Angle With Steering Voltage

## 4.0 ANTENNA DESIGN OVERVIEW

### 4.1 AIRBORNE TRANSMIT

The airborne transmit antenna uses the uplink DSCS frequency plan consisting of six channels in the band from 7.90 to 8.40 GHz. The antenna can be used to transmit any of the six channels. The design can also be used with future broadband applications where the entire 500 MHz bandwidth is used instantaneously.

Number of elements	256 (approximate)
Element layout	triangular grid, circular aperture
Array diameter	31 cm (13 in)
EIRP (at 75° scan)	47 dBWi
Polarization	circular
Conical scan range	75°
Operating frequency	7.90-8.40 GHz
Instantaneous bandwidth	<500 MHz
Mounting accommodation	E3A

Figure 4.1-1. Performance Parameters for the Airborne Transmit Antenna

The array consists of nominally 256 elements<sup>1</sup>. The elements are arranged on a triangular grid to form a circular aperture with a diameter of 35 cm (14 inches). The effective isotropic radiated power (EIRP) is +47 dBWi. The output polarization is circular. The antenna has a conical scan range of 75°. The antenna must reconfigure to maintain the communication link during maneuvers.

True-time-delay beam steering to the subarray was considered. For this application, it was determined that true time delay was not required. The beam squint loss is less than 1 dB, even for a 500 MHz instantaneous bandwidth. Future applications with larger instantaneous bandwidths or apertures will require true time delay. True time delay can be added to this architecture if required.

The antenna was originally specified to be conformal using the fuselage of an E3A as a guideline. After further study, this specification was deemed unnecessary. The array aperture is about 14 inches in diameter, and the drag penalty associated with keeping the array planar is believed to be insignificant.

---

<sup>1</sup> Throughout the design plan, the number of elements is left as approximately 256. The exact number will depend on the detailed design of the antennas, integrated optical controllers, etc., and is likely to be slightly smaller than 256. The impact of the approximation is small when considering the system performance.

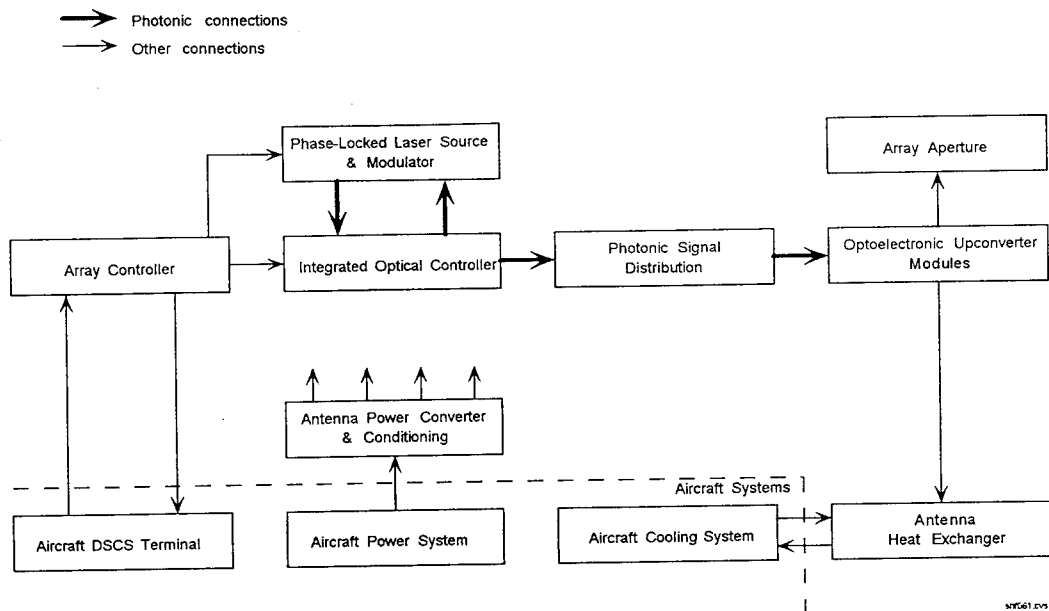


Figure 4.1-2. Airborne Transmit Antenna Block Diagram

Figure 4.1-2 shows a top level block diagram of the airborne transmit antenna. The array controller gets an IF modulation signal and scan angle settings from the aircraft DSCS terminal. The array controller uses the scan angle information to determine phase settings for the array. The phase settings are relayed to the integrated optical controller. The IF modulation signal is routed to the phase-locked laser source, where one of the optical carriers is modulated. The optical output from the phase-locked laser source is sent to the integrated optical controller. The integrated optical controller splits the optical power and applies phase and amplitude weights for each element. The photonic signal distribution network takes the weighted optical signals and conveys them to the optoelectronic upconverter modules. The upconverter modules produce complex-weighted RF signals for each element. The RF signals are sent to the array aperture where they are radiated to form the steered antenna beam. An antenna power supply converts raw power from the aircraft power system into stable DC voltages required by the various antenna blocks. The antenna heat exchanger removes waste heat from the antenna and transfers it to the aircraft cooling system. Each of the blocks in Figure 4.1-2 are discussed in more detail in the System Design Plan document.

Figure 4.1-3 shows a calculation of the airborne transmit antenna effective isotropic radiated power (EIRP). The numbers are estimates and may change slightly when the detailed antenna design is complete. The output level of each of the phase-locked lasers is +36 dBm or 4 watts. The integrated optical controller splits the two optical carriers ( $f_1$  and  $f_2$ ) 256 ways, applies amplitude and phase weights, and then combines to produce 256 outputs. The reduction in power is 24 dB for the splitting, 3 dB for the combining, and 6 dB excess loss due to propagation and interconnects. The outputs from the integrated optical controller are routed to the antenna elements through the photonic signal distribution network. The distribution network is allotted 2 dB loss due to connectors. The power level at the photodiode is then +1 dBm per laser (1.3 mW).

With the modulator in the phase-locked laser module at the optimum drive level and a photodiode responsivity of 0.8 amps/watt, the RF signal photocurrent amplitude is 1.2 mA. Assuming impedance

matching gain of 7 dB, the power delivered to the first amplifier in the optoelectronic upconverter is -7 dBm. A module gain of 40 dB yields an output power of +33 dBm (2 watts) from the RF power amplifier.

With the elements on a triangular grid having sides of length  $0.58 \lambda$ , the maximum antenna directivity is 5.6 dB. The maximum scan angle of  $75^\circ$  gives a scan loss of 5.9 dB. Another 3 dB loss is budgeted for polarization mismatch, radome loss, active impedance mismatch, etc. This yields a worst-case element gain of -3.3 dB and an element EIRP of -0.7 dBW.

If random amplitude and phase errors are held to better than 0.8 dB and  $11^\circ$ , respectively, the power loss in the main beam is less than 0.4 dB. With 256 elements, the array EIRP becomes +47 dBW.

**Optical Power Budget**

Laser #1 Output Power		36.2 dBm	4.2 W
256-way splitting loss	24.1 dB		
Integrated optical controller excess loss	6.0 dB		
2x1 combiner loss	3.0 dB		
Photonic signal distribution loss	2.0 dB		
Laser #1 Power to photodiode		1.1 dBm	1.3 mW
Laser #2 Output Power		36.2 dBm	4.2 W
256-way splitting loss	24.1 dB		
Integrated optical controller excess loss	6.0 dB		
2x1 combiner loss	3.0 dB		
Photonic signal distribution loss	2.0 dB		
Laser #2 Power to photodiode		1.1 dBm	1.3 mW
Photodiode Responsivity	0.8 A/W		
RF signal photocurrent amplitude	1.2 mA		
Impedance Matching gain	7 dB		
Power delivered to Amp	-7.4 dBm		
Amplifier Gain	40 dB		
Amplifier Output Power to Radiator		32.6 dBm	

**Element EIRP Calculation**

X-direction element spacing (triangular)	0.58 waves	
Y-direction element spacing	0.50 waves	
Antenna element directivity (4 pi dx dy)	5.6 dB	
Max scan angle	75 deg	
Scan loss (cos(theta))	5.9 dB	
Polarization mismatch, radome loss, active impedance mismatch, etc.	3 dB	
Element gain		-3.3 dB
Element EIRP		-0.7 dBW <sub>i</sub>

**Array EIRP Calculation**

Random Amplitude and Phase Error	0.3 RMS
Loss due to random errors	0.4 dB
Number of elements	256

Array EIRP	47.1 dBW <sub>i</sub>
------------	-----------------------

Figure 4.1-3. Airborne Transmit Antenna EIRP Calculation

## 4.2 AIRBORNE RECEIVE

The airborne receive antenna uses the DSCS downlink frequency plan consisting of six channels in the band from 7.25 to 7.75 GHz. The design can be used to transmit any of the six channels. The design can also be used to accommodate future broadband applications using the entire 500 MHz bandwidth instantaneously.

Number of elements	256 (approximate)
Element layout	triangular grid, circular aperture
Array diameter	37 cm (14 in)
Element noise figure	< 6 dB
G/T (at 75° scan)	-3 dB/K
Polarization	circular
Conical scan range:	75°
Operating frequency	7.25-7.75 GHz
Instantaneous bandwidth	<500 MHz
Mounting accommodation	E3A

Figure 4.2-1. Performance Parameters for the Airborne Receive Antenna

The array consists of approximately 256 elements arranged on a triangular grid in a circular aperture. The aperture has a diameter of 35 cm. The element noise figure is better than 6 dB. The array G/T is estimated to be about -3 dB/K. The receive polarization is circular. The array has a conical scan range of 75° and must be able to reconfigure to maintain the communication link during maneuvers.

As was the case for the airborne transmit array, true time delay beamsteering was not implemented because of the small fractional bandwidth and small aperture. The squint loss is less than 1 dB over the entire 500 MHz band. Future applications may require true-time delay. True time delay for the receive array could be added at the subarray level in the IF combiner, if required.

The requirement to make the array conformal to the fuselage of an E3A was also not implemented. The array diameter of 14 inches is small enough to have a negligible drag penalty.

A block diagram of the airborne receive antenna is shown in Figure 4.2-2. The array controller obtains a direction to steer the receive array from the aircraft DSCS terminal. The array controller computes a set of phase weights to form a beam in the required direction. The weights are transmitted to the integrated optical phase controller. The phase-locked laser source generates two optical carriers with a fixed frequency offset. The optical carriers are sent to the integrated optical controller. At the integrated optical controller, the optical carriers are split and the complex weights are applied. The complex-weighted outputs are transferred through the photonic distribution network to the optoelectronic downconverter modules. The optical carriers are detected in the optoelectronic downconverters to form a local oscillator signal that is mixed with the element's received RF signal. The resulting IF signals are added in the IF signal combiner to form the main array beam. The combined signal is returned to the aircraft DSCS terminal through the array controller. The antenna power supply converts raw power from the aircraft power system into stable DC voltages required by the various antenna blocks. The antenna heat exchanger

removes waste heat from the antenna and transfers it to the aircraft cooling system. Each of the blocks in Figure 4.2-2 is discussed in more detail in the System Design Plan document.

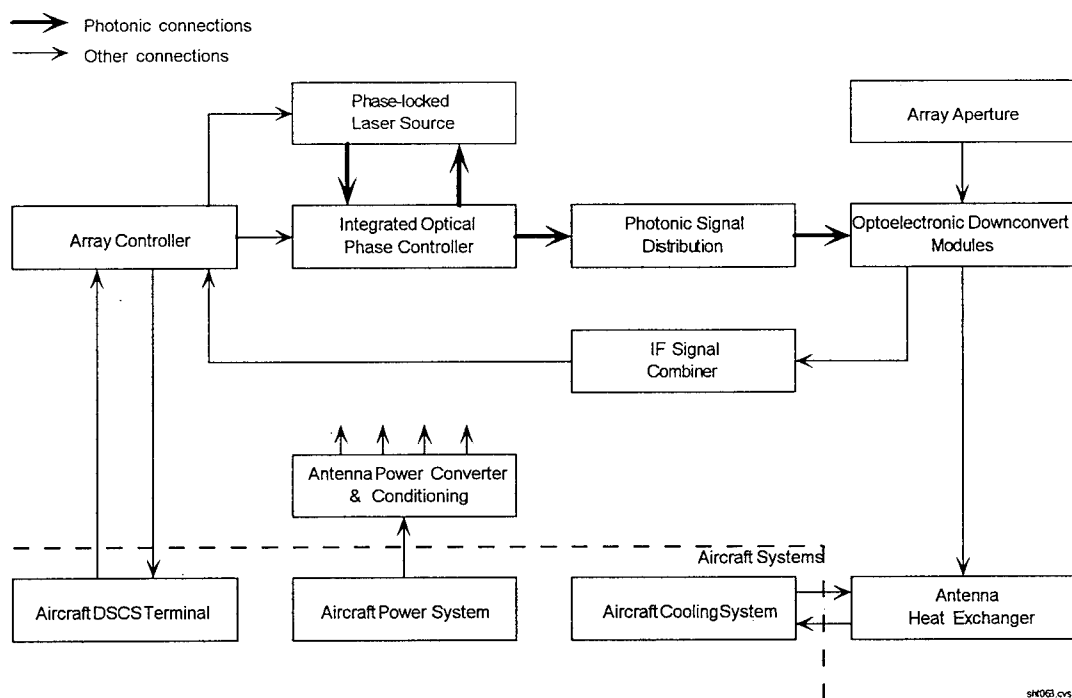


Figure 4.2-2. Airborne Receive Antenna Block Diagram

Figure 4.2-3 shows a calculation of the element noise figure and G/T for the airborne receive antenna. The element noise calculation includes components due to the galactic background radiation and terrain radiation picked up through the antenna sidelobes, the MMIC low noise amplifier (LNA), the RF mixer, the array IF combiner loss, and a second stage amplifier. The gain of the low noise amplifier is large enough to ensure that the LNA's noise dominates the total. For a 2 dB LNA noise figure, the element noise figure is estimated to be 3.3 dB. The element directivity of 5.6 dB is overcome by the losses due to the 75° scan angle, polarization mismatch, and impedance mismatch to yield a worst-case element gain of -1.1 dB. With 256 elements and 0.4 dB loss due to random amplitude and phase errors, the array G/T becomes -2.6 dB/K.



<b>Galactic, Terrain &amp; Atmospheric Temperature</b>	Tae(K)		60
<b>Element Input Losses</b>			
Polarizer and antenna element insertion loss	Lp(dB)	0.2	
Radome loss	Lr(dB)	0.1	
Module input loss	Lmin(dB)	0.2	
Temperature of element losses	T0(K)	290	
Contribution to Element Noise Temperature	T1(K)		35
<b>MMIC Low Noise Amplifier</b>			
Noise figure	Fa1(dB)	2	
Noise temperature	Ta1(K)	170	
Gain	Ga1(dB)	25	
Contribution to Element Noise Temperature	T2(K)		190
<b>Mixer and Output Loss</b>			
Mixer loss	Lps(dB)	7.5	
Module output loss	Lmout(dB)	0.6	
Array Combiner Ohmic Loss	Ln(dB)	6	
Contribution to Element Noise Temperature	T3(K)		26
<b>Second Stage Low Noise Amplifier</b>			
Noise figure	Fa2(dB)	2	
Second stage noise temperature	Ta2(K)	170	
Contribution to Element Noise Temperature	T4(K)		15
<b>Element Noise Temperature</b>	Te(K)		328
	Te(dB K)		25.2
Element Noise Figure	Fe(dB)		3.3
<b>Per Element Gain Component Description</b>			
X-direction Element Spacing	dx(waves)	0.58	
Y-direction Element Spacing	dy(waves)	0.50	
Antenna Element directivity	De(dB)	5.6	
Max Scan Angle	Theta(deg)	75	
Scan Loss	Ls(dB)	5.9	
Polarization Mismatch Loss	La(dB)	0.3	
Active Impedence Mismatch	Lv(dB)	0.5	
Element Gain	Ge(dB)		-1.1
<b>Per Element G/T</b>	Ge/Te(dB/K)		-26.2
<b>Array Component Description</b>			
Random Amplitude and Phase Errors	$\sigma$	0.3	
Loss due to amplitude and phase errors	L $\sigma$ (dB)	0.4	
Number of elements	N	256	
<b>Array G/T</b>	Ga/Ta(dB/K)		-2.6

Figure 4.2-3. Airborne Receive Antenna G/T Calculation

### 4.3 SPACE-BASED TRANSMIT

The space-based transmit antenna uses the downlink DSCS frequency plan consisting of six channels in the 7.25 to 7.75 GHz frequency band. The antenna can form up to four independent simultaneous beams. Any channel can be transmitted on any beam. Each of the four beams can be steered to anywhere on the visible earth's surface. Each of the four beams can be configured as either a full-earth-coverage beam or a spot beam.

Number of elements	256 (approximate)
Element layout	triangular grid, circular aperture
Array diameter	147 cm (58 in)
EIRP	50 dBWi per spot beam +26 dBWi for full-earth-coverage beam
Number of simultaneous beams	4
Polarization	circular
Beamwidth	spot beam or full-earth coverage
Conical scan range	9°
Operating frequency	7.25-7.75 GHz
Instantaneous bandwidth	<500 MHz
Mounting accommodation	TBD satellite

Figure 4.3-1. Performance Parameters for the Space-Based Transmit Antenna

The antenna consists of approximately 256 elements located on a triangular grid. The total aperture is circular with a diameter of 147 cm (58 inches). The EIRP is +50 dBWi per spot beam. The EIRP for a full-earth coverage beam is about +26 dBWi. The antenna has a conical scan range of 9°, which allows the spot beam to be steered anywhere on the visible earth's surface from geosynchronous orbit.

Figure 4.3-2 shows a block diagram of the space-based transmit antenna. The space-based antenna is similar to the airborne transmit antenna. The array controller receives beam direction commands and IF signals from the DSCS terminal. Element phases and amplitudes are computed and sent to the integrated optical controller. The phase-locked laser source now modulates all four IF signals onto one of the optical carriers. The integrated optical controller has four times as many amplitude and phase shifters. The photonic signal distribution network delivers the complex-weighted optical carriers to the optoelectronic upconverters. The upconverters generate the RF signals that are radiated to form the four transmit beams. A power supply and heat exchanger suitable for the spacecraft must also be designed.

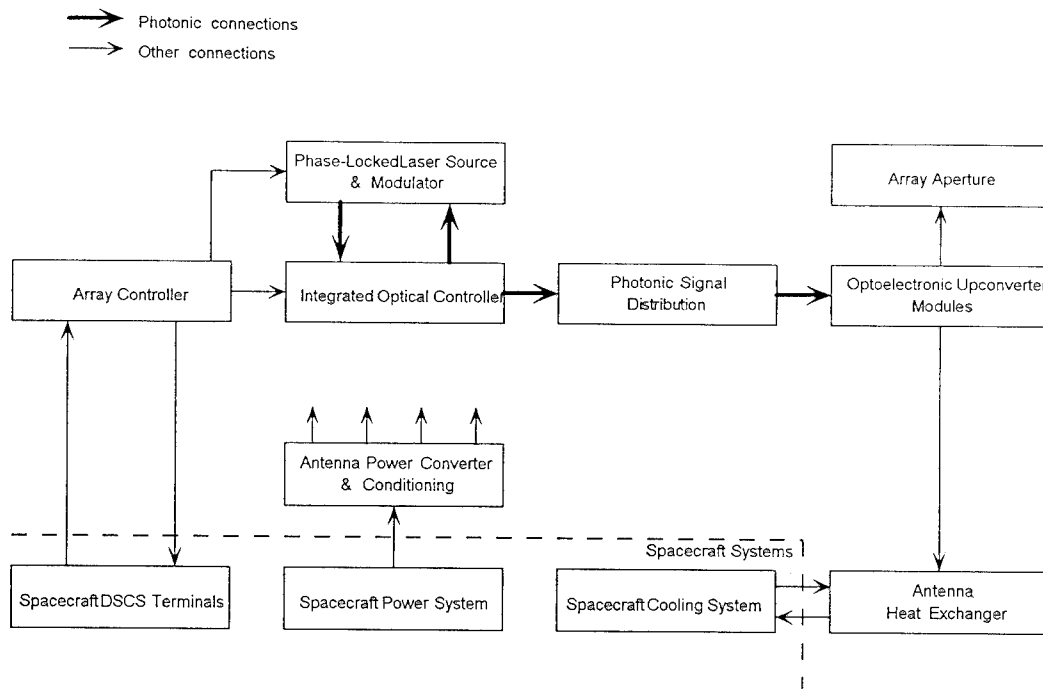


Figure 4.3-2. Space-Based Receive Antenna Block Diagram

Figure 4.3-3 shows a calculation of the EIRP of the space-based transmit antenna. The first laser has an output of 1.8 watts. This carrier sees 36 dB loss (including splitting) while passing through the integrated optical controller and photonic distribution network. Each of the four antenna beams requires 1.8 W at the second laser carrier frequency for a total of 7.2 W. The second carrier is split, complex-weighted, and combined with the first optical carrier. This process is expected to cause 42 dB of optical loss. At the photodiode, the amplitude of the desired beat signal is 0.2 mA. Including matching gain, the RF power delivered to the low-noise amplifier is -23 dBm. After 40 dB gain, the output of the amplifier is +17.2 dBm (50 mW) for each of the four beams. The power amplifier is required to operate in the linear region because four signals are processed through each element.

The  $2\lambda$ -spacing of the antenna elements gives 17.6 dB directivity. The small scan angle causes only 0.1 dB loss. Including 2 dB for polarization mismatch, impedance mismatch, etc., and 0.4 dB for random phase and amplitude errors, and 256 elements in the array yields an EIRP of +50 dBW<sub>i</sub> per spot beam.

**Optical Power Budget**

Laser #1 Output Power		32.5 dBm	1.8 W
256-way splitting loss	24.1 dB		
2x1 combiner loss	3.0 dB		
Integrated optical controller excess loss	7.0 dB		
Photonic signal distribution network loss	2.0 dB		
<hr/>			
Laser #1 Power to photodiode		-3.6 dBm	0.4 mW
Laser #2 Output Power		32.5 dBm	1.8 W
256-way splitting loss	24.1 dB		
4x1 combiner loss	6.0 dB		
2x1 combiner loss	3.0 dB		
Integrated optical controller excess loss	7.0 dB		
Photonic signal distribution network loss	2.0 dB		
<hr/>			
Laser #2 Power to photodiode		-9.6 dBm	0.11 mW
Photodiode Responsivity	0.8 A/W		
RF signal photocurrent amplitude	0.2 mA		
Impedance Matching gain	7 dB		
Power delivered to Amp	-22.8 dBm		
Amplifier Gain	40 dB		
Amplifier Output Power to Radiator		17.2 dBm	

**Element EIRP Calculation**

X-direction element spacing (triangular)	2.31 waves	
Y-direction element spacing	2.00 waves	
Antenna element directivity (4 pi dx dy)	17.6 dB	
Max scan angle	9 deg	
Scan loss (cos(theta))	0.1 dB	
Polarization mismatch,		
active impedance mismatch, etc.	2 dB	
<hr/>		
Element gain		15.6 dB
Element EIRP		2.8 dBW <sub>i</sub>

**Array EIRP Calculation**

Random Amplitude and Phase Error	0.3 RMS
Loss due to random errors	0.4 dB
Number of elements	256

Array EIRP	50.5 dBW <sub>i</sub>
------------	-----------------------

Figure 4.3-3. Space-Based Transmit Antenna EIRP Calculation

#### 4.4 SPACE-BASED RECEIVE

The space-based receive antenna uses the DSCS uplink frequency plan consisting of six channels in the band from 7.90 to 8.40 GHz. The antenna can form up to four simultaneous and independent receive beams. Any channel can be received on any of the four beams. Each of the beams can be steered to anywhere on the visible earth's surface. Each of the four beams can be configured as either a spot beam or a full-earth-coverage beam. The standard DSCS channels have a maximum instantaneous bandwidth of 85 MHz. The present design can also support future applications using the full 500 MHz DSCS bandwidth instantaneously.

Number of elements	256 (approximate)
Element layout	triangular grid, circular aperture
Array diameter	136 cm (53 in)
Element noise figure	< 6 dB
G/T (at 9° scan)	12 dB/K for spot beam -12 dB/K for full-earth-coverage beam
Number of simultaneous beams	4
Polarization	circular
Conical scan range	9°
Operating frequency	7.90-8.40 GHz
Instantaneous bandwidth	<500 MHz
Number of simultaneous jammers that can be nulled	3
Number of elements used as auxiliaries for jammer nulling	24 (six per beam)
Mounting accommodation	TBD satellite

Figure 4.4-1. Performance Parameters for the Space-Based Receive Antenna

The antenna consists of approximately 256 elements located on a triangular grid. The total aperture is circular with a diameter of 136 cm (53 inches). The element noise figure is better than 6 dB. The array G/T is 12 dB/K for a spot beam and -12 dB/K when the beam is spoiled to form a full-earth-coverage beam. The receive polarization is circular. The antenna beam can be steered up to 9° from the normal, which is enough range to reach anywhere on the visible earth's surface from geosynchronous orbit.

The space-based receive antenna has the capability to suppress up to three simultaneous broadband jammers. The signals from 24 of the antenna elements are correlated with the main antenna output to produce feedback signals for nulling jammers.

Figure 4.4-2 shows a block diagram of the space-based receive antenna. The antenna architecture is very similar to the airborne receive antenna. The spacecraft DSCS terminal sends commands to the array controller specifying the direction of each of the four beams. The DSCS terminal must also determine whether each beam is a spot beam or a full-earth-coverage beam. The array controller computes the phase weights for each of the antenna elements. A separate set of phase weights is required for each of the active receive beams. The phase-locked laser source produces two optical carriers at a fixed offset frequency.

These optical carriers are phase weighted by the integrated optical controller with the phases calculated by the array controller. The weighted optical carriers are sent to the optoelectronic downconverter modules. The downconverter modules take the received RF signals and mix them down to an intermediate frequency (IF) using the phase-weighted optical carriers as local oscillators. The IF signals are combined and returned to the spacecraft DSCS terminal through the array controller. Feedback signals for nulling jammers are obtained by correlating the output of the main array with certain auxiliary antenna elements. These correlation signals are returned to the array controller where they are used to adjust the auxiliary element phases to form a null. The space-based receive antenna also requires a power supply to provide a variety of stable voltages to the various antenna modules. A heat exchanger will be required to remove waste heat from the receive aperture.

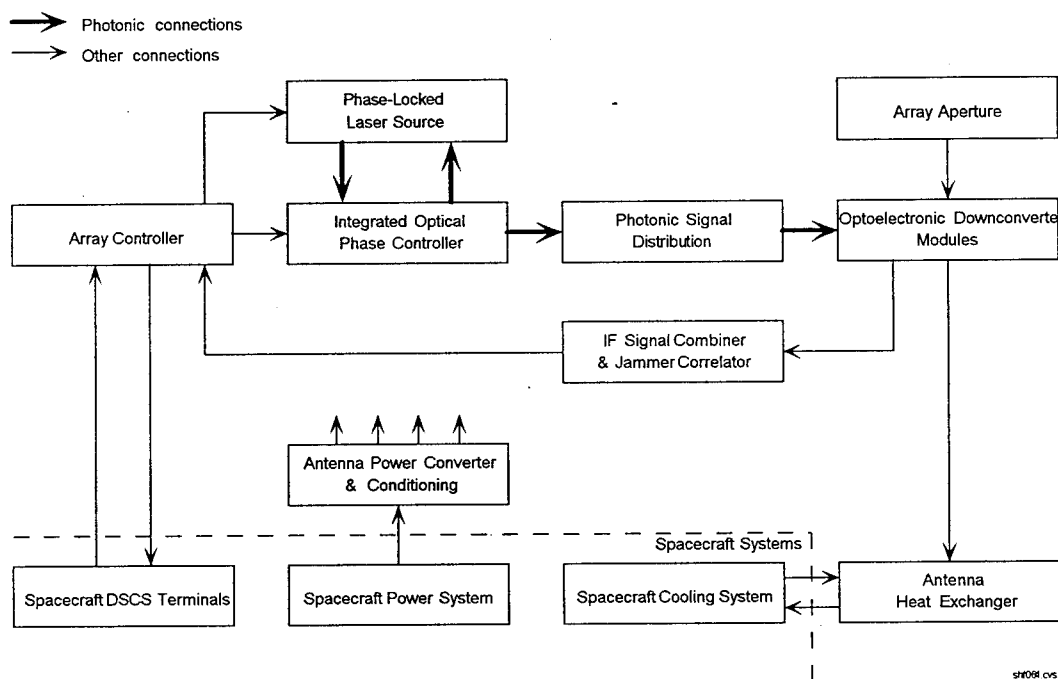


Figure 4.4-2. Space-Based Receive Antenna Block Diagram

Figure 4.4-3 shows a calculation of the element noise figure and G/T for the space-based receive antenna. The element noise temperature is dominated by background radiation from the earth. The second largest contribution is expected to come from the low-noise amplifier in the optoelectronic downconverter module. The element noise figure is estimated to be 5.1 dB. The element gain is expected to be about 17 dB because of the  $2\lambda$  element spacing and the small scan angle required from geosynchronous orbit. After including a fraction of a dB loss for random phase and amplitude errors and the array gain for 256 elements, the overall array G/T is 12.3 dB/K.

<b>Galactic, Terrain &amp; Atmospheric Temperature</b>	T <sub>ae</sub> (K)		290
<b>Element Input Losses</b>			
Polarizer and antenna element insertion loss	L <sub>p</sub> (dB)	0.2	
Module input loss	L <sub>min</sub> (dB)	0.2	
Temperature of element losses	T <sub>0</sub> (K)	290	
Contribution to Element Noise Temperature	T <sub>1</sub> (K)		28
<b>MMIC Low Noise Amplifier</b>			
Noise figure	F <sub>a1</sub> (dB)	2	
Noise temperature	T <sub>a1</sub> (K)	170	
Gain	G <sub>a1</sub> (dB)	25	
Contribution to Element Noise Temperature	T <sub>2</sub> (K)		186
<b>4-Way Split, Mixer, and Output Loss</b>			
4-way splitter loss	L <sub>sp</sub> (dB)	7	
Mixer loss	L <sub>mx</sub> (dB)	7.5	
Module output loss	L <sub>mout</sub> (dB)	0.6	
Array Combiner Ohmic Loss	L <sub>n</sub> (dB)	6	
Contribution to Element Noise Temperature	T <sub>3</sub> (K)		130
<b>Second Stage Low Noise Amplifier</b>			
Noise figure	F <sub>a2</sub> (dB)	2	
Second stage noise temperature	T <sub>a2</sub> (K)	170	
Contribution to Element Noise Temperature	T <sub>4</sub> (K)		15
<b>Element Noise Temperature</b>	T <sub>e</sub> (K)		649
	T <sub>e</sub> (dB K)		28.1
Element Noise Figure	F <sub>e</sub> (dB)		5.1
<b>Per Element Gain Component Description</b>			
X-direction Element Spacing	dx(waves)	2.3	
Y-direction Element Spacing	dy(waves)	2.0	
Antenna Element directivity	D <sub>e</sub> (dB)	17.6	
Max Scan Angle	Theta(deg)	9	
Scan Loss	L <sub>s</sub> (dB)	0.1	
Polarization Mismatch Loss	L <sub>a</sub> (dB)	0.3	
Active Impedance Mismatch	L <sub>v</sub> (dB)	0.5	
Element Gain	G <sub>e</sub> (dB)		16.8
<b>Per Element G/T</b>	G <sub>e</sub> /T <sub>e</sub> (dB/K)		-11.3
<b>Array Component Description</b>			
Random Amplitude and Phase Errors	σ	0.3	
Loss due to amplitude and phase errors	L <sub>σ</sub> (dB)	0.4	
Number of elements	N	256	
<b>Array G/T</b>	G <sub>a</sub> /T <sub>a</sub> (dB/K)		12.3

Figure 4.4-3. Space-Based Receive Antenna G/T Calculation

## 5.0 CONCLUSIONS

Photonics technology offers multiple advantages when applied to phased array antenna problems. When compared to coaxial cables or RF waveguide, there are advantages of:

- light weight,
- small size,
- low transmission loss,
- optical multiplexing,
- broad bandwidth,
- common component designs for multiple RF bands, and
- resistance to electromagnetic effects (EME).

These advantages come into play when signals must be transferred back and forth between the phased array controller and a possibly remote phased array aperture. Future systems with higher transmission frequencies, broader bandwidths, and longer transmission distances further compound the photonic advantage.

A less well known advantage of photonics technology is that it offers phased array antenna signal processing capabilities. These capabilities either are not available or are prohibitively expensive when implemented by purely electronic means. These signal processing functions include:

- high-resolution, broadband amplitude and phase control of RF signals,
- variable true-time delay, and
- broadband correlation for jammer nulling.

As an additional feature, many of these signal processing functions can be implemented so that the hardware design is independent of the actual RF antenna band. Thus, photonic signal processing module designs can be common to multiple applications, reducing system cost and increasing functionality.

This contract investigated the application of photonic technology to airborne and space-based phased array antennas compatible with the Defense Satellite Communication System (DSCS). The goal of the design was to identify areas in the phased array design where it is advantageous and practical to apply photonic technology. Areas of particular interest for the application of photonics include:

- beam forming,
- beam steering,
- beam nulling,
- data control, and
- RF signal distribution.

A conclusion resulting from this study is that photonics technology does provide the capabilities stated above for RF signal distribution and phased array antenna signal processing. Except for the space-based jammer nulling requirement, the DSCS communication application that is the focus of this study is not particularly demanding. The present-day DSCS channels have small fractional bandwidths (about 1%) and do not require true-time delay beam steering. True-time delay would be required for the airborne antenna if the instantaneous bandwidth was increased to more than about 1 GHz. The arrays do not have low sidelobe constraints and, therefore, do not require particularly tight tolerances on phase and amplitude



control. Element spacings are nearly an inch for the airborne array and even more for the space-based array, allowing ample room for conventional electronic phase and amplitude control circuits at the antenna elements.

For the DSCS application, the area where photonics technology can make the most significant contribution is with the space-based receive antenna. This antenna requires relatively tight tolerances on element phases and amplitudes in order to adapt and form deep nulls to reject unwanted jammers. Depending on the desired null depth, the required accuracies could be a few degrees of phase and a small fraction of a dB in amplitude across a channel bandwidth. Photonics technology offers the possibility of such accuracies over even broader bandwidths.

Phased array antennas with the following characteristics would increase the practicality and highlight the advantages of using photonics technology:

- large fractional bandwidths or multiband applications,
- multiple beam applications,
- large apertures,
- low sidelobe constraints,
- jammer nulling requirements, or
- extremely high RF center frequency with close element spacing.

The DSCS application considered here offers the advantage of relatively low cost hardware so that larger-scale photonically-controlled phased array antenna prototypes can be built to demonstrate the capabilities of the emerging technology. The frequency-independent nature of the integrated phase, amplitude, and true time delay control technology ensures that the results will extend to any RF band.

## 6.0 REFERENCES

1. LeComte, "Adaptive Wideband Optical Antenna Nulling System --- Final Report", Lincoln Lab Project Report SC-101, 4 August 1994.
2. White, Warren D., "Wideband Interference Cancellation in Adaptive Sidelobe Cancellers," IEEE Trans. on Aerospace and Electronic Systems, Vol. AES-19, No. 6, November 1983, pp. 915-925.
3. Mailloux, R.J., *Phased Array Antenna Handbook*, Artech House, Boston, 1994, pp. 178-182.

***MISSION***  
***OF***  
***ROME LABORATORY***

**Mission.** The mission of Rome Laboratory is to advance the science and technologies of command, control, communications and intelligence and to transition them into systems to meet customer needs. To achieve this, Rome Lab:

- a. Conducts vigorous research, development and test programs in all applicable technologies;
- b. Transitions technology to current and future systems to improve operational capability, readiness, and supportability;
- c. Provides a full range of technical support to Air Force Materiel Command product centers and other Air Force organizations;
- d. Promotes transfer of technology to the private sector;
- e. Maintains leading edge technological expertise in the areas of surveillance, communications, command and control, intelligence, reliability science, electro-magnetic technology, photonics, signal processing, and computational science.

The thrust areas of technical competence include: Surveillance, Communications, Command and Control, Intelligence, Signal Processing, Computer Science and Technology, Electromagnetic Technology, Photonics and Reliability Sciences.